Galectin-9 regulates dendritic cell contractility and migration via RhoA

Guus Franken[1], Jorge Cuenca-Escalona[1], Isabel Stehle[1], Vince van Reijmersdal[1], Rohit Gokhale[1], René Classens[1], Stefania diBlasio[1], Andrea Rodgers Furones[1], Yusuf Dolen[1], Annemiek van Spriel[1], Laia Querol Cano[1, *].

[1] Department of Medical BioSciences, Radboud University Medical Center, Geert Grooteplein 26-28, 6525 GA Nijmegen, The Netherlands.

* Corresponding author: Laia Querol Cano. Department of Medical BioSciences, Radboud University Medical Center, Geert Grooteplein 26-28, 6525 GA Nijmegen, The Netherlands. Email: Laia.QuerolCano@radboudumc.nl – Phone: + 31 24 3617600.

Acknowledgements

The authors thank the Radboudumc Technology Center Microscopy for use of their microscopy facilities. The RPPA Core is supported by NCI Grant # CA016672 and Dr. Yiling Lu's NIH R50 Grant # R50CA221675: Functional Proteomics by Reverse Phase Protein Array in Cancer. "The Functional Proteomics Reverse Phase Protein Array Core was supported in part by The University of Texas MD Anderson Cancer Center, P30CA016672, and R50CA221675." This work is supported by grants 11618 and 12949 from the Dutch Cancer Society. AvS is supported by the Netherlands Organization for Scientific Research (NWO): the Institute of Chemical Immunology (project ICI 000-23), ZonMW (project 09120012010023), and the European Research Council: Consolidator Grant (project 724281) and Proof-of-Concept Grant (project 101112687).

Abstract

To initiate adaptive immune responses, dendritic cells (DCs) migrate long distances to transport antigens from peripheral tissues to draining lymph nodes employing a so-called ameboid migration mode. Despite its critical importance, the specific molecular mechanisms that regulate DC migration are poorly characterised. Galectins, a family of β-galactoside-binding proteins, constitute a novel mechanism of membrane organisation at the cell surface and, in this way, exert crucial roles in multiple physiological and pathological processes. Nonetheless, the molecular mechanisms that underlie galectin functions are poorly described and their membrane interacting partners are mostly unknown.

Here, we report that galectin-9 is required for the dynamic behaviour and motility of DCs. We demonstrate that galectin-9 deficiency results in impaired chemokine-driven and basal DC migration both in human and mouse, suggesting a conserved function for galectin-9. Deficiency in contractility was identified as the underlying mechanism, which could be rescued by restoring membrane-bound galectin-9 levels. Furthermore, we show that galectin-9 controls RhoA activity and downstream signalling, in turn causing rearrangements of the actin cytoskeleton at the cell rear that promote DC efficient migration. Galectin-9 interaction with the adhesion receptor CD44 was required for its function enhancing DC migration. Remarkably, analysis of DC motility in a 3D environment containing a tumour spheroid revealed galectin-9 is required for DC persistent migration towards the tumour and for DC infiltration. Moreover, exogenous galectin-9 rescued the motility of immunocompromised primary blood DCs, revealing a novel role for galectin-9 in the tumour microenvironment, with potential implications for DC-based immunotherapies.

Introduction

Dendritic cells (DCs) are a major component of the immune system, linking innate and adaptive responses [1] . As professional antigen presenting cells, they take up immunogenic antigens from the site of infection or inflammation, after which they activate and undergo maturation. DC maturation triggers the upregulation of specific surface proteins such the chemokine receptor CCR7, that enables CCL19/CCL21 chemotaxis, co-stimulatory molecules like CD83 or CD86 or Major Histocompatibility Molecules (MHC) required for proper T cell activation. Mature DCs migrate to secondary lymphoid organs in a CCL19/CCL21 chemokine-directed process for antigen presentation to naive antigen-specific T cells [2-4] . Rapid DC motility is crucial for the execution of their functions and DCs, as well as other leukocytes, migrate in a so-called amoeboid manner, independent of integrins and mainly promoted by the existence of a front-rear polarity and actomyosin contractility [5]. Ameboid migration is mediated by the Rho family of small GTPases, key regulators of cytoskeletal dynamics that generate a polarised and dynamic activity balance at the front and rear of the cell [6, 7]. Most Rho GTPases rely on particular guanine nucleotide exchange factors (GEFs) and GTPase-activating proteins (GAPs) to cycle between an inactive, GDP-bound, and an active, GTP-bound form, which interacts with and activates downstream targets [8]. Illustrating this, Rac1 and Cdc42 located at the front of the cell drive filamentous actin polymerisation and directionality respectively, while RhoA at the cell rear, also called the uropod, mediates acto-myosin contractility through Rho-associated kinase (ROCK) [7, 9, 10]. Polarised migrating DCs show enrichment of integrins and intercellular adhesion molecules such as CD44 at the uropod, which link the actin cytoskeleton to the cell membrane, promoting actin polymerisation in a RhoA-dependent manner [11, 12]. However, the specific crosstalk that supports membrane amoeboid movement while connecting with intracellular events that initiate cytoskeletal rearrangements remains unresolved.

Galectins are a group of animal lectins that display a conserved affinity for β-galactoside modifications on extracellular proteins and lipids [13]. All galectins contain one or two carbohydrate recognition domains that allow them to simultaneously interact with various glycosylated binding partners, thereby modulating the clustering, surface expression and activity of a large range of cell surface proteoglycans [13-15]. Outside of their extracellular functions, many galectins are also found in the cytosol, where they establish carbohydrate-independent protein-protein interactions [13, 16, 17] and in the nucleus where they participate in mRNA splicing [18].

Galectin-9 is a ubiquitously expressed tandem-repeat galectin, which consists of two carbohydrate recognition domains joined by a linker peptide [19, 20]. It is known to exert numerous functions both intra and extracellularly and has been implicated in homeostasis and disease due to its roles in cancer, infection and inflammation[14, 21, 22]. Galectin-9 mediated effects are cell-type dependent and are dictated by the spatiotemporal expression of its binding partners. Illustrating its versatility, galectin-9 was first characterised as an eosinophil chemo-attractant [23], it induces cell death and immune tolerance by binding T cell immunoglobulin-3 in T helper 1 (T_H1) cells [24], it promotes the expansion of immunosuppressive macrophages [25] and monocytic myeloid-derived suppressor cells [26] and it has been shown to negatively regulate B cell receptor signalling [27, 28]. Contrary to these reports implicating an immunosuppressive role for galectin-9, we and others have previously identified galectin-9 to positively regulate DC biology although many of its functions in myeloid cells remain poorly defined [29-31].

A potential role of galectin-9 in migration has been mostly described for tumour cells where galectin-9 has been shown to prevent metastasis by blocking the interaction between cell membrane receptor CD44 and hyaluronic acid in the extracellular matrix [32]. Similarly, neutrophil adhesion promoted by galectin-9 was shown to be mediated by CD44 binding [33], which in turn enhances RhoA expression and activation [11, 34]. Galectin-9 is a known binding partner of

CD44, being able to block interaction with its ligand hyaluronan [35]. However, the mechanism(s) by which galectin-9 mediates DC motility are not delineated. We have recently reported intracellular galectin-9 to be involved in regulating actin cytoskeleton reorganisation and stabilising the plasma membrane in DCs [30]. In addition, dengue virus-infected DCs were shown to up-regulate galectin-9 expression and their ability to migrate towards CCL19 and CXCL12 cytokines [36].

Here, we show galectin-9 is required for optimal basal as well as chemokine-driven DC migration *in vitro* and *in vivo*, indicating an evolutionary conserved function. Specifically, we highlight a uropod retraction defect upon galectin-9 depletion, which we relate to reduced active RhoA and its downstream signalling, as the underlying mechanism. Importantly, restoring galectin-9 expression is sufficient to recover cell contractility via its interaction with CD44. Highlighting the physiological relevance of our findings, we demonstrate a role for galectin-9 in rescuing the migration of immunosuppressed DCs, suggesting a role for galectin-9 in the tumour microenvironment.

Materials and Methods

Generation of monocyte-derived dendritic cells

Dendritic cells were derived from peripheral blood monocytes isolated from a buffy coat (Sanquin, Nijmegen, The Netherlands) [37]. Monocytes isolated from healthy blood donors (informed consent obtained) were cultured for up to five days in RPMI 1640 medium (Life Technologies, Bleiswijk, Netherlands) containing 10 % foetal bovine serum (FBS, Greiner Bio-one, Alphen aan den Rijn, Netherlands), 1 mM ultra-glutamine (BioWhittaker), antibiotics (100 U/ml penicillin, 100 µg/ml streptomycin and 0.25 µg/ml amphotericin B, Life Technologies), IL-4 (500 U/ml) and GM-CSF (800 U/ml, #130-093-868, Miltenyi Biotec) in a humidified, 5 % CO_2. On day 3, moDCs were supplemented with new IL-4 (500 U/ml, Miltenyi) and GM-CSF (800 U/ml, Miltenyi). On day 6, moDCs were supplemented with a maturation cocktail: IL-6 (15 ng/ml, #130-093-933, Miltenyi Biotec), TNF-α (10 ng/mg, #130-094-014 Miltenyi Biotec), IL-1β (5 ng/m, #130-093-898 Miltenyi Biotec) and PGE2 (10 ug/ml, Pfizer). When necessary, moDCs were treated with recombinant galectin-9 protein (AF2045, R&D systems) at a final concentration of 1 µg/ml.

Isolation and culture of primary cells

Human cDC2s were isolated from peripheral blood mononuclear cells derived from healthy individuals (Sanquin, Nijmegen, the Netherlands) using the MACS CD1c+ isolation kit (130-119-475, Miltenyi Biotec) according to manufacturer's instructions. Cell purity was determined by flow cytometry (see Figure S6A) using antibodies specific against CD20-FITC (1:100 345792, BD Biosciences), CD14-PerCP (1:50, 325632, Biolegend), CD11c-APC (1:50 559877, BD Biosciences) and CD1c-PE (1:50, #130-113-302, Miletnyi Biotec). After isolation, fresh cDC2s were cultured in X-VIVO-15 (Lonza) supplemented with 2 % human serum (HS, Sigma-Aldrich) at a concentration of $0.5x10^6$ cells/ml. cDC2s were matured overnight as previously described with a maturation cocktail (MC) composed of 50 U/ml GM-CSF, 100 U/ml IL-6, 100 U/ml IL-1β, 50 U/ml TNFα (50 U/ml and 200 nM of PGE2. Next day, cDC2s were harvested, washed, and replated in media composed of 50 % fresh X-VIVO-15 supplemented with 2 % HS and 50 % melanoma cell line A375 derived conditioned media (CM) for 24 hours. When necessary, 1 µg/ml of recombinant galectin-9 was provided for the final 2 hours of cDC2 coculture with melanoma-derived CM. Next, cDC2s were harvested and washed prior to further analysis.

For BMDCs, bone marrow was taken from the tibias and femurs of 9-week-old C57BL/6 Lgals9 -/- mice or wild type litter mates and cultured in RPMI containing 10 % FBS and 3 % granulocyte macrophage colony-stimulating factor (mGM-CSF) (Peprotech). for 7 days. Cells were treated with 1 µg/ml LPS for 16 h prior to being used.

Cell culture, generation of tumour spheroids and conditioned media preparation

The melanoma cells MEL624 and BLM were cultured in Gibco DMEM high glucose medium (Life Technologies) supplemented with 10 % FBS and 0.5 % antibiotics (100 U/ml penicillin, 100 µg/ml streptomycin and 0.25 µg/ml amphotericin B, Life Technologies). A375 melanoma cell line was cultured in DMEM (high glucose, GlutaMAX, Gibco) and further supplemented with 10% FBS (HyClone) and 1% antibiotic-antimycotic (Gibco). To generate tumour spheroids cells were harvested using PBS containing 0.25 % trypsin and 4 mM EDTA and collected in Gibco DMEM high glucose medium (Life Technologies) containing 10 % FBS. For spheroid production. Tumour cells were cultured in 30 µl droplets containing 4000 tumour cells resuspended in spheroid medium (60 % growth medium and 40 % low viscosity methyl cellulose medium (25cp viscosity; Sigma Life Science), to which 3.6 µl of PureCol Type I Collagen (3.1 mg/ml stock solution; Advanced Biomatrix) was added.

To obtain melanoma-derived CM, A375 cells were seeded at a cell concentration of 0.25 x10^6 cells/ml. After 72 hours, A375 CM was harvested and centrifuged at 1500 rpms for 5 minutes to get rid of cellular debris and frozen until further use.

Small interfering RNA knockdown

On day 3 of DC differentiation, cells were harvested and subjected to electroporation. Three custom stealth small interfering RNA (siRNA) were used to silence galectin-9 (LGALS9HSS142807, LGALS9HSS142808 and LGALS9HSS142809) (Invitrogen). Equal amounts of the siRNA ON-TARGETplus non-targeting (NT) siRNA#1 (Thermo Scientific) were used as control. Cells were washed twice in PBS and once in OptiMEM without phenol red (Invitrogen). A total of 15 µg siRNA (5 µg from each siRNA) was transferred to a 4-mm cuvette (Bio-Rad) and 5-10x10^6 DCs were added in 200 µl OptiMEM and incubated for 3 min before being pulsed with an exponential decay pulse at 300 V, 150 mF, in a Genepulser Xcell (Bio-Rad, Veenendaal, Netherlands), as previously described [29, 30]. Immediately after electroporation, cells were transferred to preheated (37 °C) phenol red–free RPMI 1640 culture medium supplemented with 1 % ultraglutamine, 10 % (v/v) FCS, IL-4 (300 U/ml), and GM-CSF (450 U/ml) and seeded at a final density of 5x10^5 cells/ml.

Chemotaxis assays

Day 6 mature NT or *Lgals9* siRNA transfected moDCs (1x10^5 cells in 50 µl) were seeded in the top chamber of a 24-well transwell containing a polycarbonate filter of 5 µm pore size (Corning; #CLS3421). 550 µl of RPMI medium supplemented with 1 µg/ml recombinant human CCL21 (BioLegend; #582208) or nothing as negative control were added to the lower chambers. Plates were incubated for the specified time points at 37 °C, 5 % CO_2 after which migrated cells in the bottom chamber were collected and acquired on a MACSQuant Analyzer 10 Flow Cytometer using the MACSQuantify software (Miltenyi Biotec). The percentage of specific migration was calculated by dividing the number of cells migrated to the lower well by the total cell input (50 µl cell suspension directly measured on the MACSQuant Flow Cytometer).

Chemotactic assays using cDC2s were performed using the transwell 96-well plate 5 µm pore size (CLS3388-2EA). 3x10^4 cDC2s were seeded in the top chamber of the transwell. Lower compartment of the transwell plate was loaded with 200 µl of X-VIVO-15 supplemented with 2 % HS and 100 ng/ml of CCL19 and CCL21 (#582102, #582202, Biolegend). To determine passive cDC2 migration, media without CCL19 nor CCL21 was used. Plate was incubated for 3 hours at 37 °C, 5 % CO_2 after which migrated cells in the bottom chamber were collected and acquired on a MACSQuant Analyzer 10 Flow Cytometer together with the initially loaded cDC2s for each condition. Percentage of cDC2 migration was assessed by dividing the number of migrated cDC2s by the number of initially loaded cDC2s for each condition. Relative cDC2 migration was determined by dividing the percentage of migrated cDC2s of each condition by the percentage of migrated mature cDC2s unexposed to melanoma-derived CM x 100.

3D migration assays

A collagen mixture was generated using *PureCol*® Type I Bovine Collagen Solution (Advanced Biomatrix, final concentration 1.7 mg/ml), α-modified minimal essential medium (Sigma Albrich) and sodium bicarbonate. Collagen mixture was allowed to pre-polymerise for 5 minutes at 37 °C prior to adding a 45 µl cell suspension containing 30.000 mature day 8 NT or *Lgals9* siRNA transfected moDCs in phenol red–free RPMI 1640 culture medium supplemented with

1 % ultraglutamine and 10 % FBS. The total mixture (100 µl/well) was transferred to a 96-well black plate (Greiner Bio-One; #655090) and incubated for 45 minutes at 37 °C to allow collagen polimerisation. Afterwards, 100 µl of phenol red–free RPMI 1640 culture medium supplemented with 1 % ultraglutamine and 10 % FBS was added on top of the matrices. When appropriate, galectin-9 depleted moDCs were pre-treated with 1 µg/ml recombinant galectin-9 for 3, 24 or 48 h prior to being embedded into the collagen gel. For some experiments NT and *Lgals9* siRNA transfected moDCs were treated with 10 µg/ml of the anti-CD44 blocking antibody [33] for 30 min prior to being embedded into the collagen gel. When relevant, moDC cell suspension was mixed with one tumour spheroid prior to being added to the collagen matrix and the microscopy plate was inverted after every 7-10 minutes during collagen polymerisation to prevent the spheroid from sinking into the matrix. In collagen gels containing tumour spheroid moDCs were stained with PKH-26 (Sigma Albrich) or CellTrace CFSE (Invitrogen) according to manufacturer's instructions and to distinguish them from tumour cells.

Time-lapsed video microscopy was performed using the BD Pathway 855 spinning disk confocal microscope (BD Bioscience), the atto vision software (BD Bioscience) and the 10X objective (Olympus). Sequential images were acquired every 4-5 minutes for 10 hours using the 548/20 excitation filter (Chroma), emission filter 84101 (Chroma) and dichroic filter 84000 (Chroma). When appropriate, time-lapse microscopy was performed using the Celldiscoverer7 (Zeiss), using the 5x objective with 2x tube lens or the the BD Pathway 855 spinning disk confocal microscope (BD Bioscience), the atto vision software (BD Bioscience) and the 10X objective (Olympus). Sequential images were acquired every 4-5 minutes for 10 hours using the 548/20 excitation filter (Chroma), emission filter 84101 (Chroma) and dichroic filter 84000 (Chroma). Time-lapse sequences were analysed with the ImageJ manual-tracking plugin to measure cell velocity and to track individual cells.

In vivo adoptive transfer

Wild type and galectin-9$^{-/-}$ DCs were labelled with 5 µM carboxyfluorescein succinimidyl exter (CFSE) violet and far-red dyes following manufacturer's instructions (Invitrogen; #C34571 and C34572 respectively), mixed in equal numbers (1x10^{6} each in 50 µl) and co-injected into the same footpad or tail vein of either wild type or galectin-9$^{-/-}$ recipient mice. Donor DCs arriving in the draining lymph node (popliteal and inguinal respectively) were enumerated 48 h later by flow cytometry using a BD FACSLyric flow cytometer (BD BioSciences).

Reverse phase protein array (RPPA)

Cellular proteins were denatured in a 1 % SDS + 2-mercaptoethanol buffer solution and diluted in five 2- fold serial dilutions in dilution lysis buffer. Serially diluted lysates were arrayed on nitrocellulose-coated slides (Grace Bio-Labs) by the Quanterix (Aushon) 2470 Arrayer (Quanterix Corporation) and each slide was probed with a validated primary antibody plus a biotin-conjugated secondary antibody (https://www.mdanderson.org/research/research-resources/core-facilities/functional-proteomics-rppacore/antibody-information-and-protocols.html). Signal detection was amplified using an Agilent GenPoint staining platform (Agilent Technologies) and visualized by DAB colorimetric reaction. The slides were scanned (Huron TissueScope, Huron Digital Pathology) and quantified using customized software (Array-Pro Analyzer, Media Cybernetics) to generate spot intensity. Relative protein level for each sample was determined by RPPA SPACE [38] (developed by MD Anderson Department of Bioinformatics and Computational Biology, https://bioinformatics.mdanderson.org/public-software/rppaspace/). The protein concentrations of each set of slides were then normalized for protein loading. Correction factor was calculated by (1) median-centring across samples of

all antibody experiments; and (2) median centring across antibodies for each sample. Results were then normalized across RPPA sets by replicates-based normalization as described [39]. Details of the RPPA platform as performed by the RPPA Core are described in [40]. Pathway enrichment analysis was performed using the metascape platform and the analysis outlined in [41].

Flow cytometry

To determine depletion of galectin-9 following siRNA transfection, single cell suspensions were stained with a goat anti-galectin-9 antibody (AF2045, R&D systems) at 8 µg/ml or isotype control as negative control for 30 min at 4 °C. Before staining, moDCs cells were incubated with 2 % human serum for 10 min on ice to block non-specific interaction of the antibodies with FcRs. A donkey-anti goat secondary antibody conjugated to Alexa Fluor 488 was used (Invitrogen; 1:400 (v/v).

moDCs were incubated for 30 min on ice with antibodies against HLA-DR (BD BioSciences; # 555811, clone G46-6, FITC-labelled), CD80 (BD BioSciences; # 557227, clone C3H, PE-labelled), CD86 (BD BioSciences; #555658, clone 2331, PE-labelled), CD83 (Miltenyi; # 130-094-186, clone HB15, APC-labelled), CCR7 (#130-094-286, Miltenyi Biotec). All antibodies were used at a final 1:25 (v/v) dilution in cold PBS containing 0.1 % BSA, 0.01 % NaH_3 (PBA) supplemented with2 % HS.

To phenotype cDC2s, harvested cDC2s were first blocked in PBA buffer supplemented with 2 % HS for 15 minutes. After blocking, cDC2s were stained in PBA buffer with anti-galectin-9 antibody (1:50, AF2045, R&D systems) and anti-CCR7 (1:200) for 20 minutes. Next, cells were washed and stained with a secondary antibody, a donkey-anti-goat antibody conjugated to Alexa488 (1:400, Invitrogen) for 20 minutes. Stained cDC2s were analysed by flow cytometry using a FACS Verse and later analysed using FlowJo software (BD, Franklin lakes, NJ, USA).

RhoA pull down

2–3x10^6 day 6 WT, galectin-9 KD or galectin-9 rDCs were collected. RhoA GTPase activity was measured using the RhoA Pull-Down Activation Assay Biochem Kit (#BK036; Cytoskeleton) according to the manufacturer's instructions. Active RhoA protein was quantified using the Image Studio Lite software (Li-Cor).

Western Blot

Day 6 moDCs were lysed in lysis buffer for 30 min on ice prior to being spun down at 10.000 rpm for 5 min. The BCA protein assay (Pierce, ThermoFisher scientific) was conducted to determine protein concentration and following manufacturer's instructions and for each sample, 20 µg of total protein were diluted using SDS sample buffer (62.5 mM Tris pH 6.8, 2 % SDS, 10 % glycerol).

Proteins were separated by SDS-PAGE and blotted onto PVDF membranes. Membranes were blocked in TBS containing 3 % BSA at room temperature for 1 h prior to be stained with specific antibodies. Antibody signals were detected with HRP coupled secondary antibodies and developed using Odyssey CLx (Li-Cor) following manufacturer's instructions. Images were retrieved using the Image Studio Lite 5.0 software. The following primary antibodies were used for Western Blotting: goat anti-Galectin-9 (AF2045, R&D systems, Minneapolis, Minnesota) at 1:1000 (v/v), rabbit anti-phospho(Thr 423) Pak1 (#2601; Cell Signaling Technology) at 1:500 (v/v), rabbit anti-Pak1 (#2602; Cell Signaling Technology) at 1:500 (v/v), rabbit anti-GAPDH (#2118; Cell Signaling Technology) at 1:500 (v/v), mouse anti-phospho myosin light chain (#3675, Cell Signaling Technology) at 1:500 (v/v), mouse anti-mDia (#610848, BD BioSciences) at

1:500 (v/v) and rat anti-tubulin (Novus Biological, Abingdon, United Kingdom) at 1:2000 (v/v). The following secondary antibodies were used: donkey anti-goat IRDye 680 (920-32224, Li-Cor, Lincoln, Nebraska), donkey anti-rabbit IRDye 800 (926-32213, Li-Cor), donkey anti rabbit IRDye 680 (926-68073, Li-Cor), goat anti rabbit IRDye 800 (926-32211, LiCor), goat anti-rat IRDye 680 (A21096, Invitrogen, Landsmeer, Netherlands), donkey anti-mouse IRDye 680 (926-68072, Li-Cor). All secondary antibodies were used at 1:5000 (v/v).

Data analysis

Cell tracking was performed using the manual tracking plugin of Fiji (ImageJ) with adjusted microscope-specific time and calibration parameters. Individual cells were tracked for at least 90 minutes 5 hours after being embedded in the collagen to allow adaptation to the environment. The mean square displacement (MS) over time intervals was determined as previously described [42]. In short, the MSD was calculated per time interval for each cell. The average per time interval was calculated for all cells corrected for the tracking length of the cells. The Euclidean distance reached by a cell after 60 minutes of tracking with respect to their starting position was calculated using the Chemotaxis and Migration software (Ibidi) after adjusting the X/Y calibration and time acquisition interval. Tracking plots were generated using the Chemotaxis and Migration software (Ibidi).

For the pathway enrichment analysis, we identified the top 50 genes correlating with *lgals9* gene across all immune cells using the ULI RNA-seq dataset (GSE109125) and the gene constellation tool from the Immunological Genome Project (ImmGen). We then conducted a functional pathway enrichment analysis using gProfiler [43] accross the Reactome dataset [44].

All data was processed using Excel 2019 (Microsoft) and plotted using GraphPad Prism 8 software. All statistical analysis was done using Prism 8. All data is expressed as mean ± SEM unless otherwise stated. The statistical test used to analyse each data set is described in the corresponding figure legend. Unpaired t- test was used to compare mean values between NT and *gal9* siRNA transfected cells. one-way analysis of variance (ANOVA) was used for multiple comparison. cDC2 data was analysed using one-way analysis of variance (ANOVA) followed by a Dunnett's test for multiple comparison. Statistical significance was considered for p values < 0.05.

Results

Galectin-9 is required for dendritic cell migration

Dendritic cells quickly migrate long distances to transport antigen from peripheral tissues to lymph nodes, a process indispensable for the initiation of immune responses. Actin polymerisation regulates three-dimensional migration speed in DCs [45]. Our discovery that galectin-9 is highly enriched in membrane structures in DCs and that it mediates actin contractility [30] prompted us to study its involvement in governing DC migration. To this end, we investigated the functional consequences of galectin-9 depletion for DC migration using non-targeting siRNA transfected and *Lgals9* siRNA-transfected moDCs (herewith referred to as WT and galectin-9 KD DCs respectively). Galectin-9 expression is almost completely inhibited by this approach (Figure S1A and S1B) while analysis of the maturation makers (HLA-DR, CD80, CD83 and CD86) showed a similar upregulation upon DC maturation for both WT and galectin-9 KD DCs (Figure S1C and S1D) demonstrating no impairment in DC maturation upon galectin-9 depletion. DC migration is primarily guided by the chemokines CCL19 and CCL21 that bind the CC-chemokine receptor 7 (CCR7), which is upregulated in DCs upon activation [46]. We first analysed chemokine-driven migration towards CCL21 using a transwell chamber containing a collagen gel. The presence of CCL21 induced DC migration through the transwell membranes in both WT and galectin-9 KD DCs but this was significantly decreased in the latter for all donors analysed (Figure 1A and 1B). Concomitantly, DCs were shown to be trapped in the collagen gel upon galectin-9 depletion (Figure S2A and S2B) demonstrating an involvement of galectin-9 in chemokine-driven DC migration. We obtained a similar phenotype when DCs were subjected to CCL21 gradient in the absence of collagen (Figure S2C and S2D) and also in this setup a marked reduction in DC migration was obtained when galectin-9 was depleted. Importantly, the migration defect cannot be attributed to the aberrant expression of the chemokine receptor CCR7 (Figure S1E) as this was found to be equally expressed in WT and galectin-9 KD DCs. Next, we moved to in-depth study the effect of galectin-9 in three-dimensional (3D) migration and characterised the movement of individual WT and galectin-9 depleted DCs embedded in collagen gels using life cell imaging microscopy. Using the ImageJ plug-in for manual tracking we detected that the average migratory speed (velocity), mean square displacement (MSD) and Euclidean distance were significantly diminished in galectin-9 KD DCS (Figure 1C, 1D, 1E and 1F). Individual cell tracks from WT and galectin-9-depleted DCs clearly illustrate how galectin-9 KD DCs fail to migrate within the 3D collagen matrix away from their initial location and highlight the impairment in 3D motility upon galectin-9 depletion (Figure 1G). We also performed 3D collagen migration assays containing a melanoma tumour spheroid embedded within the collagen matrix to investigate how galectin-9 depletion alters DC function in the tumour microenvironment (Figure 2A and 2B). Time-lapsed video microscopy analysis of individual cells demonstrated that also in this context, galectin-9 depletion resulted in a significant decrease in their velocity of approximately 40 % compared to WT DCs (average speed of 4.1 µm/min in WT to 2.4 µm/min in gal-9 KD DCs) (Figure 2C) as well as their MSD and Euclidean distance (Figure 2D and 2E). This effect was not cell-line specific as 3D assays performed with another melanoma line (BLM) yielded similar results (Figure S3A and S3B). Interestingly, mature WT DCs enhanced their migratory capacity in the presence of a tumour spheroid and this increase was only marginal in galectin-9 KD DCs, suggesting that lack of galectin-9 impairs the capacity of DCs to respond to stimuli (Figure S3C-S3E).

Next, we sought to investigate whether galectin-9 function in DC migration was evolutionarily conserved using *in situ* migration assays on WT and *galectin-9* $^{-/-}$ bone marrow derived DCs (BMDC). First, transwell assays were performed using a gradient of murine CCL21 and as previously observed for human DCs, lack of galectin-9 also impaired the migration of murine DCs (Figure 3A). Next, WT and galectin-9 knockout (KO) DCs were labelled with far-red and

violet carboxyfluorescein succinimidyl ester (CFSE) dyes, mixed in equal numbers and co-injected into the same footpad or tail vein. Donor DCs arriving in the draining popliteal and inguinal lymph nodes respectively were enumerated 48 h later via flow cytometry (Figure 3B and 3C). The percentage and total numbers of migratory *galectin-9*$^{-/-}$ BMDCs were significantly reduced compared to WT DCs irrespective of the host genotype (galectin-9 WT or KO) (Figure 3D). Similar results were obtained in experiments in which violet-labelled WT and far-red galectin-9 KO BMDCs were employed, ruling out any specific effect of the fluorescent dyes on migration (Figure 3E).

We have previously published galectin-9 exists both in an extracellular (membrane-bound) as well as in a cytosolic fraction in DCs [30]. To gain further insights into the molecular mechanism underlying galectin-9 involvement in DC migration we cultured galectin-9 KD DCs with exogenous galectin-9 protein (gal-9 KD +rGal9 DCs) to restore surface-bound levels of galectin-9 (Figure 4A), embedded WT, galectin-9 KD and gal-9 KD +rGal9 DCs in 3D collagen matrices and determined their migration ability. Restoring galectin-9 levels rescued the migration impairment observed in galectin-9 KD DCs for all donors analysed and no differences were observed in the velocity or the mean square displacement between WT and gal-9 KD +rGal9 DCs (Figure 4B and 4C respectively). Moreover, individual cell tracks illustrate the ability of DCs to migrate upon restoring galectin-9 levels as these cells are indistinguishable from the WT counterparts (Figure 4D). Interestingly, exogenous addition of galectin-9 rescued DC migration also after short incubations confirming the fundamental role of galectin-9 in driving DC migration and suggesting surface-bound galectin-9 drives DC migration as shorter incubations may not allow sufficient galectin-9 internalisation and potential intracellular activity (Figure S4A and S4B). Interestingly, and in stark contrast to what was observed in basal 3D migration assays, the presence of a tumour spheroid rendered gal-9 KD +rGal9 DCs unable to migrate adequately and no rescue in their cell velocity was observed compared to galectin-9 KD in this setting (Figure 4E and S4C). Similarly, replenishing the surface pool of galectin-9 did not rescue the ability of DCs to infiltrate a tumour spheroid and, as observed for galectin-9 KD DCs, we failed to find gal-9 KD +rGal9 DCs either inside the tumour spheroid or in the surrounding area (Figure 4F and S4D respectively).

Overall, our results show that galectin-9 is required for both basal and chemokine-directed migration in DCs and that this function appears to be evolutionarily conserved.

Galectin-9 controls RhoA-mediated contractility in dendritic cells.

Leukocytes are known to follow the so-called “amoeboid migration” mode in which cell movement is driven by protrusive flowing of the anterior actin network followed by actomyosin contractility of the trailing edge (also called uropod) [5]. To mechanistically understand how galectin-9 dictates DC migration we morphologically characterised migratory WT, galectin-9 KD and gal-9 KD +rGal9 DCs in a 3D collagen matrix and observed a striking difference in their ability to retract the cell rear. Motility of WT cells is characterised by a shrinkage of the uropod with concomitant forward movement (supplementary movie 1 and Figure 5A). Galectin-9 depleted DCs displayed a delay in their ability to contract the cell rear, which was therefore visible for longer periods of time during contractile phases (Supplementary movie 2, Figure 5A and 5B). Remarkably, addition of exogenous galectin-9 protein rescued DC contractility and the uropod was no longer detected for abnormal lengths of time in gal-9 KD +rGal9 DCs (Supplementary movie 3, Figure 5A and 5B). Interestingly, DC elongation was not found to differ between WT, galectin-9 KD or gal-9 KD +rGal9 DCs (Figure 5C) implying that galectin-9 does not permanently alter cellular shape or length but the impairment in uropod retraction is rather due to the inability to timely contract the cell rear. Anterograde protrusion at the cell front is functionally dissociated from the retrograde contractility forces that mediate uropod retraction [5]and no differences

were observed in the leading-edge protrusion formation suggesting galectin-9 is not involved in this process (data not shown).

RhoA signalling mediates uropod contraction at the trailing edge [6, 47] and thus we next examined if RhoA-mediated signalling was altered upon galectin-9 depletion. Although total RhoA levels did not differ between WT, galectin-9 KD and gal-9 KD +rGal9 DCs (Figure 5D) RhoA GTPase activity was markedly decreased in galectin-9 KD DCs (Figure 5E), which is in agreement with the aforementioned impairment in uropod retraction.

Reverse phase protein array (RPPA) [40] performed against more than 450 key functional proteins on WT, galectin-9 KD and gal-9 KD +rGal9 DCs whole lysates revealed a striking decline in either protein expression or activity in galectin-9 KD cells compared to WT or gal-9 KD +rGal9 DCs (Figure 6A). Remarkably, treatment with exogenous galectin-9 protein rescued DC signalling signature as only minimal differences in protein expression were detected between WT and gal-9 KD +rGal9 DCs (Figure 6A). Enrichment pathway analysis performed [41] on the differentially expressed proteins confirmed galectin-9 is a positive regulator of cell motility (Figure 6B). Validating our analysis, cytokine signalling was also found to be positively regulated in WT compared to galectin-9 KD DCs, which we have previously reported [29]. RPPA analysis revealed that the active form of P21 activated kinase 1 (PAK1) (PAK_Thr423), an activating Ser/Thr kinase downstream of RhoA, is downregulated in galectin-9 KD DCs whereas treatment with exogenous galectin-9 protein (gal-9 KD +rGal9 DCs) rescues its levels to those found in WT cells. Interestingly, total levels of PAK1 did not differ across samples suggesting galectin-9 is not involved in regulating its expression. Analysis of phosphorylated and total PAK1 levels in multiple donors validated our RPPA data and confirmed PAK to be differentially regulated in response to galectin-9 cellular levels (Figure 6C and 6D). Interestingly, we did not see any differences in other downstream RhoA signalling molecules (mDia and phosphomyosin light chain (PiMLC) (Figure 6D) upon galectin-9 depletion or over-expression suggesting galectin-9 regulates RhoA-mediated contractility by mechanisms that are independent of MLC phosphorylation.

To further confirm the link between galectin-9 and RhoA, we sought to investigate which genes positively correlate with *lgals9* expression and the pathways they mediate. We obtained a list of the top 50 genes correlating with *lgals9* using the ULI RNA-seq dataset (GSE109125) from the Immunological Genome Project (ImmGen) and performed a functional pathway enrichment analysis using the Reactome dataset [44] (Figure S5A). Data obtained showed a significant enrichment in both the Rho GTPase Effectors and signalling by Rho GTPases pathways confirming a correlation between galectin-9 and RhoA activity (Figure S5B). Our evidence supports the conclusion that galectin-9 regulates cell rear contractility by modulating RhoA retrograde activity and Pak1-mediated downstream signalling.

We next set to unravel the molecular mechanisms by which membrane-bound galectin-9 modulates RhoA activity at the cytosol thereby regulating actin polymerisation and contractility in DCs. The transmembrane adhesion protein CD44 has been shown to interact with galectin-9 in T cells and Natural Killer cells [48, 49] and we identified CD44 to be an interacting galectin-9 binding partner in moDCs [29]. Furthermore, CD44 interacts with RhoA via its cytoplasmic tail and its spatial organisation is determined by the dynamic remodelling of the actin cytoskeleton. To characterise the functional interaction between CD44 and galectin-9 we treated WT DCs or gal-9 KD +rGal9 DCs with a blocking antibody that prevents binding of galectin-9 to CD44 [33]. Pre-incubation of gal-9 KD +rGal9 DCs with anti-CD44 blocking antibody markedly decreased the ability of recombinant galectin-9 to promote moDC migration (Figure 7A and 7B) without altering CD44 surface expression (Figure 7C). Similarly, CD44 levels were not affected by galectin-9 depletion or overexpression (Figure 7C). Interestingly, treating WT moDCs with anti-CD44 had only a marginal effect on cell migration which may indicate a differential effect of intracellular and membrane-bound galectin-9 in DC motility.

Galectin-9 is sufficient to rescue migration in tumour-immunocompromised primary DCs.

Tumour antigen collection and subsequent DC trafficking from the tumour site to lymph node structures is crucial for the effective induction of anti-tumour T cell responses [50]. However, the suppressive tumour microenvironment is known to foster DC dysfunction, impeding among others DC recruitment into the lymph nodes and subsequent launching of T cell immunity [51, 52], enabling tumour progression. To further validate the importance of galectin-9 on DC migration in a model that better recapitulates a physiological setup, the human DC subset cDC2s was used. Mature cDC2s were treated with melanoma-derived CM to impair their migratory capacity, after which galectin-9 was provided to assess its ability to rescue cDC2 migration (Figure 8A). DC homing towards lymphoid structures is dependent on the interaction between CCR7-expressing DCs and the chemokines CCL19 and CCL21. Migratory capacity of DCs was determined in a transwell migration assay towards the chemokines CCL19 and CCL21 for three hours (Figure 8B). Exposure of mature cDC2s to melanoma-derived CM led to the downregulation of surface galectin-9 and CCR7 expression levels (Figure 8C and 8D). In line with the phenotype data, tumour-primed cDC2s exhibited a lower migratory capacity towards the chemokines CCL19 and CCL21 compared to untreated mature cDC2s (Figure 8E). Remarkably, addition of exogenous galectin-9 rescued cDC2 migration towards the chemokines CCL19 and CCL21 (Figure 8E). CCR7 expression levels remained unchanged during galectin-9 addition (Figure 8D and Figure S6B), indicating this superior migratory capacity to be dependent on galectin-9 presence and not on an altered CCR7 expression. Taken together, these results validate the relevance of galectin-9 for the migration capacity of naturally occurring DC subsets in the here used tumour model and illustrates the therapeutic value of intervening galectin-9 signalling axis to restore the migration of tumour-immunocompromised DCs.

Discussion

Single cell migration is an almost ubiquitous phenomenon in mammalian cell biology with cells mostly displaying either a mesenchymal or an ameboid migration mode. The latter is employed by leukocytes, including dendritic cells (DCs), and allows for a rapid and autonomous migration, independent of adhesions to the extracellular environment. This is essential to rapidly shuttle antigens from the primary sites of infection to lymphoid organs, where adaptive immune responses are generated, and is driven by cortical actin polymerisation and actomyosin contractility forces.

In this study, we explored in depth the role of galectin-9, a tandem repeat member of the galectin family, in DC migration and report a novel function in controlling rear actin contractility via its functional interaction with CD44 at the DC surface that in turn regulates RhoA cytosolic activity. Depletion of galectin-9 significantly reduced basal and chemokine-driven migration in human and murine DCs, suggesting an evolutionary conserved function for galectin-9. We have also resolved the underlying mechanism, namely an impairment in actomyosin contractility at the cell rear, also known as the uropod. Interestingly, restoring galectin-9 surface levels using exogenous recombinant protein rescued 3D migration velocity in the absence of any stimulation but failed to restore DC migration in the presence of a tumour spheroid, suggesting galectin-9 plays multiple roles in DC migration.

Galectins bind to β-galactosides present in LacNAc of N- and O-glycans and are currently recognised as important membrane organisers thereby contributing to immune cell functioning [14, 53]. Interestingly, they are also abundantly expressed intracellularly and we and others have reported several members of the galectin family to modulate immune cell function via carbohydrate-independent interactions [17, 30]. Galectin-9 exhibits immunoregulatory effects through which it interferes with the function of various types of immune cells [24, 25, 27, 54]. Membrane protein expression and glycosylation determine the immune-mediating effect of galectin-9 [21] and in this manner, it acts as an immune suppressor in B and T cell biology while we and others have reported an stimulatory function for galectin-9 in DCs either in a glycan-dependent or independent manner. For instance, addition of recombinant galectin-9 induced the maturation of DCs [31] and we have shown galectin-9 depletion decreased DC-mediated phagocytosis and cytokine secretion [29, 30].

Galectin-9 is involved in regulating adhesion of tumour cells and immune cells via its association with various adhesion receptors like CD44 or integrins [49, 55]. Furthermore, galectin-9 expression levels positively correlate with metastasis inhibition in a number of malignancies [32, 56-58]. Interestingly, exogenous galectin-3 and -8 reduced tumour cell migration indicating that different galectins exert distinct functions and that their mechanisms of action might be cell specific [59, 60]. Similarly, galectin-3 and -9 promote leukocyte extravasation from blood into tissues under inflammatory conditions by functioning as chemoattractants while galectin-1 was found to specifically inhibit immunogenic DC extravasation into sites of inflammation [61-63]. Our findings demonstrate that galectin-9 regulates immature and mature DC basal and chemokine-driven migration suggesting an influence in general processes behind DC motility. Galectin-9 depletion does not affect DC maturation as the upregulation of various maturation markers was not different in WT versus galectin-9 depleted DCs indicating a defect in cell maturation cannot explain the impairment in migration upon galectin-9 depletion. In agreement with our data, dengue-infected DCs were shown to upregulate galectin-9, which was accompanied by an increased cell motility and galectin-9 depletion in dengue-infected DCs diminished DC motility in chemotaxis transwell assays [36]. Here, we have also uncovered a role for galectin-9 in naïve DC migration, which underlies the general relevance of galectin-9 in the context of multiple immunological settings. Furthermore, we show that galectin-9 depletion caused a defect in uropod contractility. Concomitantly, the active GTP-

bound fraction of RhoA was diminished in galectin-9 KD DCs compared to wild type counterparts, providing the basis for the observed uropod retraction defect in galectin-9 KD cells. Interestingly, the activity of RhoA-downstream targets like Pak1 was found to correlate with galectin-9 levels but no differences in expression or activity were observed for other proteins involved in RhoA signalling like piMLC or mDia suggesting a specific regulation of the Pak pathway by galectin-9-dependent interactions [64]. Pak1 is involved in cytoskeletal remodelling and phosphorylation at Thr423 activates Pak1 and is mediated by Rac1, Cdc42, and RhoA signalling [64-66]. Decreased phosphorylation at this site indicates a lack of RhoA activity, and in general a decreased polarised state of galectin-9 KD cells. Interestingly, our analysis of publicly available datasets confirmed a correlation between RhoA-related pathways and galectin-9 and a study examining migration in NK cells also reported an increase in RhoA transcript levels upon rgal9 treatment, suggesting that galectin-9 control over RhoA signalling is conserved across immune cell types [67].

Interestingly, treatment with recombinant galectin-9 protein was sufficient to rescue the defect in uropod retraction in DC basal 3D migration. Although we cannot discard that some of the exogenous protein is internalised and cytosolically active, the rescue observed in the cell movement already after very short treatment times would suggest that the surface-bound pool of galectin-9 is responsible for driving DC migration. Based on our findings, we postulate that the mechanistic link between extracellular galectin-9 and DC migration is through the formation of galectin-9-mediated functional domains on the DC membrane that enable proper downstream RhoA signalling crucial for leukocyte propulsion. Supporting this hypothesis, galectin-9 promoted T_H2 migration through matrigel by inducing protein disulfide isomerase (PDI) surface retention and, in that way, modulate integrin CD61 activity [68]. Similarly, galectin-9 enhanced neutrophil adhesion via the regulation of integrin (CD11b and CD18) activity at the cell membrane as a result of its interaction with the transmembrane adhesion receptor CD44 [33]. CD44 is located to uropods in migrating cells and is directly linked to RhoA via its cytosolic tail [11]. Moreover, CD44 can modulate RhoA activity and its downstream signalling molecule Pak1 via the activation of the RhoA guanine nucleotide-exchange-factors (GEFs) p115RhoGEF and leukemia-associated Rho guanine nucleotide exchange factor (LARG) [34, 69]. Galectin-9 has been shown to interact with and crosslink CD44 in various immune cell types and in that manner regulate cell adhesion to the CD44 ligand hyaluronic acid [33, 48, 49]. Our experiments blocking galectin-9 interaction with CD44 abrogated the migration rescue observed upon restoring the levels of galectin-9 at the DC surface, indicating that recombinant galectin-9 might regulate DC motility by binding CD44 at the DC plasma membrane. Interestingly, blocking CD44 interaction with galectin-9 in wild type DCs did not impair cell movement implying that other mechanisms might be altered upon galectin-9 depletion that result in impaired migration. This could be either surface-mediated but independent of CD44 or mediated by the intracellular pool of galectin-9.

In agreement with our results obtained in DC migration in the absence of any stimulus, mature galectin-9 depleted DCs also displayed an impaired motility capacity in a tumour microenvironment, obtained by creating tumour spheroids from melanoma cell lines and incubating them with DCs in a 3D matrix. The involvement of galectin-9 in DC migration in the tumour microenvironment has scarcely been addressed even though galectin-9 expression is recognised as a positive prognostic biomarker in various cancer types such as breast cancer, cervical squamous cell carcinoma and melanoma [70, 71]. Confirming a role for galectin-9 in the tumour microenvironment, treating primary human tumour-immunosuppressed cDC2 cells with exogenous recombinant galectin-9 rescued cell chemotactic migration in all donors analysed, indicating the importance of galectin-9 for migration in naturally occurring DC subsets, and its ability to overcome a melanoma-mediated immunosuppressed environment.

Strikingly, treatment with recombinant galectin-9 rescued DC 3D basal motility but failed to restore cell migration in the presence of a tumour spheroid. Concomitantly, tumour infiltration of DCs treated with exogenous galectin-9 was found to be similar to that of galectin-9 depleted DCs. This data suggests that either (1) the tumour spheroid secretome is inhibiting the function of recombinant galectin-9 protein at the surface of DCs or (2) intracellular galectin-9, which remains largely depleted after treatment with exogenous protein, is also relevant in DC migration. If the latter, it would imply that migrational velocity and directionality might not be necessarily linked and would open the possibility that galectin-9 functions in more than one mechanism, with migrational velocity and directionality being independently affected. Supporting this hypothesis, data obtained in the amoeboid cell migration model *Dictyostelium discoideum* suggests that cell velocity and directionality can be independently regulated by two separate signalling pathways [72]. This limited rescue ability of recombinant galectin-9 could have parallels with a previous study, where adding recombinant galectin-3 to galectin-3 KD non-small cell lung cancer cells did not rescue their migrational phenotype [73]. It is also worth mentioning that endogenous galectin-9 protein is highly susceptible to being cleaved in solution and therefore the commercial recombinant galectin-9 we use has a shortened linker for additional stability. It is possible that this change affects the binding or cross-linking abilities of recombinant galectin-9 thus failing to recapitulate all the endogenous functions.

Taken together, our study indicates the importance of galectin-9 in DC basal and directed migration towards lymph nodes and tumours. Furthermore, we provide for the first time evidence that galectin-9 regulates cell polarity and uropod contraction, namely by modulating RhoA activation in response to CD44 binding. Our data also indicates that galectin-9 controls DC migration in a glycan-dependent as well as independent manner with each pool exerting distinct roles that are not interchangeable. Lastly, data presented here highlights a role for galectin-9 in the tumour microenvironment and opens up future research avenues exploiting galectin-9 as a target in DC-mediated anti-tumour immunity.

Figure legends

Figure 1. Galectin-9 depletion reduces dendritic cell migration. A. day 3 moDCs were transfected with either a *Lgals9* siRNA or a non-targeting (NT) siRNA as negative control, matured at day 6 using a cytokine cocktail for 48 h further and subjected to a chemokine migration assay in the presence or absence of chemokine CCL21 and using a transwell orverlaid with collagen matrix. Representative flow graphs from the migratory moDC fraction are shown. **B.** Quantification of donors shown in (A). Data shows the percentage of moDCs that migrated relative to input. Each symbol represents moDCs from one donor. **C.** moDCs were treated as per (A) and embedded within a 3D collagen matrix. The mean cell velocity of a representative donor is shown. **D – F.** Mean ± SEM cell velocity (D), mean square displacement (MSD) (E) and Euclidean distance (F) of four independent donors. Twenty cells were analysed per donor and transfection. Lines in (D) connect matched NT and *Lgals9* siRNA transfected moDCs. Graph in F depicts relative Euclidean distance in *Lgals9* siRNA transfected moDCs after 60 minutes of tracking with respect to control cells. A one-way t-test was performed. **E.** Individual trajectory plots of NT and *Lgals9* siRNA transfected moDCs of one representative donor out of four analysed. End points of tracks are indicated by black dots. The black line indicates the overall movement in x and y direction (µm). Unpaired students t-test was conducted to compare NT siRNA and *Lgals9* siRNA transfected cells. * $p < 0.05$; *** $p < 0.0001$.

Figure 2. Migration of mature DCs within the tumour microenvironment is impaired upon galectin-9 depletion. A. Schematic representation of the experimental setup used for the 3D collagen gel migration assays with a melanoma tumour spheroid embedded in it. **B.** Representative single cell tracking paths of WT (NT siRNA) or galectin-9 KD (*Lgals9* siRNA) moDC embedded in a 3D collagen matrix together with a Mel624 malignant melanoma spheroid. Images were taken every 5 minutes and dots indicate cell position at the specified time point whereas lines represent the tracking path covered by each cell from their initial position at the start of the tracking (0 min). Due to microscopy limitations, the position of the spheroid in the *Lgals9* siRNA condition was outside the imaged area and is marked by a plus sign. **C.** The cell velocity, the mean square displacement **(D)** and the Euclidean distance migrated after one hour **(E)** are depicted. Data represents mean value ± SEM of three independent donors. In (C) lines connect matched NT and *Lgals9* siRNA transfected moDCs. Unpaired students t-test was performed between *Lgals9* and NT siRNA-transfected moDCs. * $p < 0.05$; ** $p < 0.01$; *** $p < 0.001$. Euclidean distance is depicted as the mean value for galectin-9 depleted moDCs relative to the control group after 60 minutes of tracking. A one-way t-test was performed. ** $p < 0.005$.

Figure 3. Galectin-9 function in dendritic cell migration is conserved in vivo. A. Bone marrow derived dendritic cells (BMDCs) obtained from either wild type (WT) or galectin-null (galectin-9 $^{-/-}$) mice were subjected to a chemokine transwell assay in the presence or absence of chemokine CCL21. Data shows the percentage of moDCs that migrated relative to input. **B.** WT and galectin-9 $^{-/-}$ BMDCs were stained with far-red or violet CFSE dyes, mixed in equal numbers and injected into the footdpat or tail vein of donor mice. Forty eight hours later draining lymph nodes were isolated and donor BMDCs enumerated by flow cytometry. **C.** Representative flow cytometry plots depicting the cellular mixtures injected into recipient mice. In mixture A, WT BMDC were stained with far-red CFSE and galectin-9 $^{-/-}$ cells received violet CFSE. For mixture B, colours were interchanged to discard any effect of the dye in cell migration. **D** and **E.** Dendritic cell mixtures from (C) were injected into WT (D) and galectin-9 KO (E) host mice. Data depicts percentage of migratory donor BMDCs ± SEM. Each symbol represents values obtained for one draining lymph node.

Figure 4. Dendritic cell migration relies on membrane-bound galectin-9 fraction. A. moDCs were transfected with *Lgals9* siRNA or a non-targeting siRNA (NT). Forty-eight hours after transfection, galectin-9 knockdown (galectin-9 KD) cells were treated with 1 µg/ml recombinant galectin-9 protein (gal-9 KD +rGal9) or nothing as negative control for 24-48 h. Surface only (left) and total (right) galectin-9 knockdown and treatment with exogenous protein were confirmed by flow cytometry 48 h after transfection. Grey population = NT siRNA (WT); red population = galectin-9 KD; green population = gal-9 KD +rGal9; dotted line = isotype control. Numbers in inset indicate geometrical mean fluorescence intensity (gMFI). **B** and **C.** moDCs treated as per (A) were embedded in 3D collagen matrices followed by live cell imaging to individually track cell migration. At least twenty cells were analysed for each donor and transfection or treatment. **B.** Violin plot showing average cell velocity of five individual donors. Each symbol represents one independent donor and lines connect paired donors. **C.** Mean square displacement was calculated and graph shows mean ± SEM of five individual donors. **D.** Individual trajectories of WT, galectin-9 KD and gal-9 KD +rGal9 moDCs. End points of tracks are indicated by red dots. Data shows representative donor of 5 analysed. **E.** moDCs treated as per (A) were embedded in 3D collagen matrices containing a melanoma tumour spheroid or nothing as control. Cell velocity was calculated and graph shows mean ± SEM of a representative donor. **F.** Collagen matrices from (E) were fixed, stained for actin and a DC marker and the number of infiltrated DCs measured for the same tumour spheroid Z plane across conditions. Graph shows mean ± SEM of two independent donors. One-Way ANOVA test with a Bonferroni post-test correction was conducted between WT, galectin-9 KD and gal-9 KD +rGal9 moDC conditions. n.s. = $p > 0.05$, * = $p < 0.05$; ** = $p < 0.005$.

Figure 5. Galectin-9 regulates uropod contractility. A. Time-lapse sequence of a representative WT DC, galectin-9 KD DC and gal-9 KD +rGal9 moDCs migrating in a 3D collagen gel. **B.** Duration of uropod presence (min) in WT DC, galectin-9 KD DC and gal-9 KD + rDC moDCs. **C.** Average cell elongation factor in WT DC, galectin-9 KD DC and gal-9 KD +rGal9 moDCs. Graphs depict mean ± SEM for four independent donors. Each symbol represents one independent donor. At least twenty cells were analysed for each donor and condition. One-Way ANOVA test with a Bonferroni post-test correction was conducted between WT DC, galectin-9 KD DC and gal-9 KD +rGal9 moDCs conditions. **D.** Total lysates from WT, galectin-9 KD and gal-9 KD +rGal9 moDCs were subjected to Western Blot and galectin-9 and total RhoA expression analysed. Tubulin was used as loading control. Immunoblot is representative of four independent experiments. **E.** Levels of active (GTP-bound) RhoA in WT DC and galectin-9 KD moDCs detected by immunoblotting. Rhotekin beads alone were used as negative control. n.s. = $p > 0.05$, * = $p < 0.05$, ** = $p < 0.01$.

Figure 6. RhoA downstream signalling is impaired in galectin-9 depleted DCs. A. Heat map of the proteins found to be differentially regulated between WT, galectin-9 KD (gal9 KD) and galectin-9 KD treated with recombinant protein (gal9 KD + rGal9) by RPPA. A total of 191 out of 486 proteins analysed were found to be altered in gal9 KD and/or gal9 KD + rGal9 conditions compared to WT control moDCs. **B.** Metascape pathway enrichment analysis performed using data shown in (A) for WT and galectin-9 KD moDCs. **C.** Total lysates from WT, galectin-9 KD and gal-9 KD +rGal9 moDCs were subjected to Western Blot and total PAK1/2, PAK_Thr423, galectin-9 expression analysed. Tubulin was used as loading control. Immunoblot is representative of two independent experiments. Graph shows quantification of PAK_Thr423 and total PAK content normalised to tubulin in each sample using ImageJ. Graph shows mean ± SEM of two independent donors. **D.** Total lysates from WT, galectin-9 KD and gal-9 KD +rGal9 moDCs were subjected to Western Blot and mDia, phosphomyosin light chain (piMLC) and galectin-9 expression analysed. Tubulin was used as loading control.

Immunoblot is representative of four independent experiments. **E.** Quantification of mDia and piMLC content normalised to tubulin in each sample using ImageJ. Graph shows mean ± SEM of four independent donors.

Figure 7. Galectin-9 interaction with CD44 regulates DC migration. A. moDCs were transfected with *Lgals9* siRNA or a non-targeting siRNA (NT). Forty-eight hours after transfection, galectin-9 knockdown (galectin-9 KD) cells were treated with 10 µg/ml of an anti-CD44 blocking antibody for 30 min prior to being treated with 1 µg/ml recombinant galectin-9 protein (gal-9 KD +rGal9 moDCs) or nothing as negative control for further 30 min. moDCs were embedded in 3D collagen matrices followed by live cell imaging to individually track cell migration and individual cell velocity calculated. Graphs show mean ± SEM of one representative donor. **B.** Mean ± SEM cell velocity of two independent donors. At least twenty cells were analysed for each donor and transfection or treatment.

Figure 8. Galectin-9 restores chemokine-driven cDC2 migration. A. Schematic representation of the experimental setup. Primary human cDC2s were matured overnight with a maturation cocktail (MC) for 24 h prior to being harvested and replated in the presence of melanoma-derived conditioned medium (CM) for 24 h. Exogenous galectin-9 was supplemented for the last 2 h of cDC2 incubation with melanoma-derived CM. Tumour-primed cDC2s were collected and analysed for the surface expression levels of galectin-9 and CCR7 or for their migratory capacity. **B.** Schematic representation of the transwell migration assay. cDC2 were seeded in the top chamber of a transwell chamber containing a 5 µm porus membrane and subjected to a chemokine gradient of the CCR7-ligands CCL19 and CCL21. Migratory cDC2s were collected after 3 h and quantified. **C.** Histograms showing the surface expression of galectin-9 and CCR7 of a representative cDC2 donor analysed by flow cytometry. **D.** Percentage of positive cDC2s for galectin-9 and CCR7 for each of the indicated treatments. **E.** Relative cDC2 migration under each treatment determined by normalising each treatment to the migration given by mature cDC2s unexposed to the melanoma-derived CM for every donor. Violin plots in (D) and (E) show mean of five independent donors. One-way ANOVA followed by Dunnett's test for multiple comparison was performed. * $p < 0.05$; ** $p < 0.01$; *** $p < 0.001$.

Supplementary Figure 1. Galectin-9 depletion does not affect dendritic cell maturation. A. Day 3 moDCs were transfected with *Lgals9* siRNA or a NT siRNA. Levels of galectin-9 were assessed by flow cytometry 48 h after transfection. Flow cytometry graph shows galectin-9 levels at the plasma membrane. Graph is representative for one donor and numbers in inset indicate geometric mean fluorescence intensity (gMFI). NT siRNA (light grey population), *Lgals9* siRNA-transfected moDCs (red population). Black dotted line represents isotype control values. **B.** Total lysates from NT and *Lgals9* siRNA transfected cells were treated with maturation cocktail or nothing, subjected to Western Blot and galectin-9 expression analysed. GAPDH was used as loading control. Immunoblot is representative of four independent experiments. **C** and **D.** NT or *Lgals9* siRNA transfected moDCs were matured and levels of HLA-DR, CD80, CD86 and CD83 analysed by flow cytometry. Graph depicts mean ± SEM surface protein levels (gMFI) of four independent donors. **E.** Membrane levels of CCR7 were assessed by flow cytometry in moDCs treated as per (C). Graph is representative for one donor of three analysed and numbers in inset indicate geometric mean fluorescence intensity (gMFI). NT siRNA (light grey population), *Lgals9* siRNA-transfected moDCs (red population). Black dotted line represents isotype control values.

Supplementary Figure 2. Galectin-9 depletion impairs chemokine-driven migration in dendritic cells. A. *Lgals9* or NT siRNA transfected moDCs were treated with maturation cocktail for 48 h prior to being stained with PKH26 and seeded on top of a collagen layer overlaying a transwell chamber with a 5 µm pore size membrane subjected to a CCL21 chemokine gradient. Cells were left to migrate for 24 h after which collagen gels were fixed and imaged by confocal microscopy. **B.** Quantification of PKH signal in WT and galectin-9 KD DC containing collagens for the total length of the collagen gel as well as the upper and lower fraction. **C.** moDCs treated as per A were placed in the upper chamber of a transwell system and subjected to a CCL21 chemokine gradient. Migrated cells were collected at the bottom chamber 1, 2 and 4 h after seeding and measured by flow cytometry. Graphs show representative donor of 4 independent donors analysed. **D.** Quantification of data shown in (C). Graph shows mean ± SEM percentage (%) of migratory DCs relative to total number of seeded cells for each time point and genotype.

Supplementary Figure 3. Galectin-9 depletion diminishes dendritic cell 3D migration. A and **B.** WT or galectin-9 depleted moDCs were matured and embedded within a 3D collagen matrix containing either a MEL624 or a BLM melanoma cell spheroids. The median cell velocity (A) and the mean square displacement (MSD) (B) were calculated. Data represents the mean value ± SEM of a representative donor. At least twenty cells were analysed per condition and genotype. **C – E.** Day 3, moDCs were transfected with either a NT or a *Lgals9* siRNA, matured or not and embedded in a collagen matrix containing a MEL624 tumour spheroid. The migration pattern of either immature (at day 6 of DC differentiation), mature (at day 8) and mature cells in the presence of a tumour spheroid (at day 8) was analysed for one representative donor. The median cell velocity (C), the MSD (D) and the Euclidean distance reached after 60 minutes of tracking (E) were assessed. Graphs represent the mean value ± SEM of one representative donor. At least twenty-five cells were analysed per condition. Unpaired student's t test was performed to compare NT and *Lgals9* siRNA transfected moDCs. n.s. $p > 0.05$; * $p < 0.05$; ** $p< 0.01$; *** $p< 0.001$.

Supplementary Figure 4. Treatment with recombinant galectin-9 protein restores dendritic cell migration. A. WT, galectin-9 KD and galectin-9 KD moDCs treated with 1 µg/ml recombinant galectin-9 protein (gal-9 KD +rGal9 moDCs) for either 3, 24 or 48 h were embedded in a 3D collagen matrix and their velocity calculated. Graph depicts average velocity ± SEM for one representative donor out of 4 analysed. **B.** Individual trajectory plots of cells shown in (A). End points of tracks are indicated by black dots. One way ANOVA with a Kruskal-Wallis for multiple comparison test was performed. n.s. $p > 0.05$; * $p < 0.05$; *** $p< 0.001$. **C.** WT, galectin-9 KD or galectin-9 KD treated with recombinant galectin-9 for 3 h moDCs were embedded in 3D collagen matrices containing a melanoma tumour spheroid or nothing as control. Accumulated distance was calculated and graph shows mean ± SEM of a representative donor. **D.** Collagen matrices from (E) were fixed, stained for actin and a DC marker and the number of DCs surrounded the spheroid measured for the same tumour spheroid Z plane across conditions. Graph shows mean ± SEM of two independent donors. Images are representative of the tumour spheroid and surrounding DCs for all three conditions analysed.

Supplementary Figure 5. RhoGTPase-mediated pathways positively correlate with *lgals9* expression. A. 50 genes that positively correlated to *lgals9* gene across all immune cell types (GSE109125 dataset) grouped by secondary correlation. **B.** Functional pathway enrichment analysis (Reactome dataset). Data is shown as $-\log_{10}$ of the adjusted p-value.

Supplementary Figure 6. cDC2 cell purity and supplementary phenotype analysis. A. Gating strategy to determine cDC2 purity after isolation from PBMCs. cDC2s were stained for CD1c, CD11c, CD14 and CD20. A first gate is set based on the physical FCS-A/SSC-A parameters followed by selecting on negative cells for CD14 and CD19. cDC2s are then identified as positive cells for CD11c and CD1c. **B.** Surface galectin-9 and CCR7 expression in galectin-9 and CCR7 positive cDC2s. Graph shows average ± SEM geometric mean fluorescence intensity (gMFI) of 5 individual donors. One-way ANOVA followed by Dunnett's test for multiple comparison was performed. * $p < 0.05$; ** $p < 0.01$; *** $p < 0.001$.

References

1. Banchereau, J., and Steinman, R. M. (1998) Dendritic cells and the control of immunity, *Nature 392*, 245-252.
2. Acton, S. E., Astarita, J. L., Malhotra, D., Lukacs-Kornek, V., Franz, B., Hess, P. R., Jakus, Z., Kuligowski, M., Fletcher, A. L., Elpek, K. G., Bellemare-Pelletier, A., Sceats, L., Reynoso, E. D., Gonzalez, S. F., Graham, D. B., Chang, J., Peters, A., Woodruff, M., Kim, Y. A., Swat, W., Morita, T., Kuchroo, V., Carroll, M. C., Kahn, M. L., Wucherpfennig, K. W., and Turley, S. J. (2012) Podoplanin-rich stromal networks induce dendritic cell motility via activation of the C-type lectin receptor CLEC-2, *Immunity 37*, 276-289.
3. Randolph, G. J., Angeli, V., and Swartz, M. A. (2005) Dendritic-cell trafficking to lymph nodes through lymphatic vessels, *Nature reviews. Immunology 5*, 617-628.
4. Wculek, S. K., Cueto, F. J., Mujal, A. M., Melero, I., Krummel, M. F., and Sancho, D. (2020) Dendritic cells in cancer immunology and immunotherapy, *Nature reviews. Immunology 20,* 7-24.
5. Lammermann, T., Bader, B. L., Monkley, S. J., Worbs, T., Wedlich-Soldner, R., Hirsch, K., Keller, M., Forster, R., Critchley, D. R., Fassler, R., and Sixt, M. (2008) Rapid leukocyte migration by integrin-independent flowing and squeezing, *Nature 453*, 51-55.
6. Hind, L. E., Vincent, W. J., and Huttenlocher, A. (2016) Leading from the Back: The Role of the Uropod in Neutrophil Polarization and Migration, *Developmental cell 38*, 161-169.
7. Sanchez-Madrid, F., and Serrador, J. M. (2009) Bringing up the rear: defining the roles of the uropod, *Nature reviews. Molecular cell biology 10*, 353-359.
8. Heasman, S. J., and Ridley, A. J. (2010) Multiple roles for RhoA during T cell transendothelial migration, *Small GTPases 1*, 174-179.
9. Wong, K., Pertz, O., Hahn, K., and Bourne, H. (2006) Neutrophil polarization: spatiotemporal dynamics of RhoA activity support a self-organizing mechanism, *Proceedings of the National Academy of Sciences of the United States of America 103*, 3639-3644.
10. Lammermann, T., Renkawitz, J., Wu, X., Hirsch, K., Brakebusch, C., and Sixt, M. (2009) Cdc42-dependent leading edge coordination is essential for interstitial dendritic cell migration, *Blood 113*, 5703-5710.
11. Zhang, Y., Xia, H., Ge, X., Chen, Q., Yuan, D., Chen, Q., Leng, W., Chen, L., Tang, Q., and Bi, F. (2014) CD44 acts through RhoA to regulate YAP signaling, *Cellular signalling 26*, 2504-2513.
12. Bourguignon, L. Y., Singleton, P. A., Zhu, H., and Diedrich, F. (2003) Hyaluronan-mediated CD44 interaction with RhoGEF and Rho kinase promotes Grb2-associated binder-1 phosphorylation and phosphatidylinositol 3-kinase signaling leading to cytokine (macrophage-colony stimulating factor) production and breast tumor progression, *The Journal of biological chemistry 278*, 29420-29434.
13. Johannes, L., Jacob, R., and Leffler, H. (2018) Galectins at a glance, *Journal of cell science 131*.
14. Liu, F. T., and Stowell, S. R. (2023) The role of galectins in immunity and infection, *Nature reviews. Immunology 23*, 479-494.
15. Querol Cano, L., Dunlock, V. E., Schwerdtfeger, F., and van Spriel, A. B. (2023) Membrane organization by tetraspanins and galectins shapes lymphocyte function, *Nature reviews. Immunology*.
16. Hong, M. H., Weng, I. C., Li, F. Y., Lin, W. H., and Liu, F. T. (2021) Intracellular galectins sense cytosolically exposed glycans as danger and mediate cellular responses, *Journal of biomedical science 28*, 16.
17. Liu, F. T., Patterson, R. J., and Wang, J. L. (2002) Intracellular functions of galectins, *Biochimica et biophysica acta 1572*, 263-273.
18. Coppin, L., Vincent, A., Frenois, F., Duchene, B., Lahdaoui, F., Stechly, L., Renaud, F., Villenet, C., Van Seuningen, I., Leteurtre, E., Dion, J., Grandjean, C., Poirier, F., Figeac, M., Delacour, D., Porchet, N., and Pigny, P. (2017) Galectin-3 is a non-classic RNA binding protein that stabilizes the mucin MUC4 mRNA in the cytoplasm of cancer cells, *Scientific reports 7*, 43927.
19. Tureci, O., Schmitt, H., Fadle, N., Pfreundschuh, M., and Sahin, U. (1997) Molecular definition of a novel human galectin which is immunogenic in patients with Hodgkin's disease, *The Journal of biological chemistry 272*, 6416-6422.
20. Leffler, H., Carlsson, S., Hedlund, M., Qian, Y., and Poirier, F. (2002) Introduction to galectins, *Glycoconjugate journal 19*, 433-440.
21. John, S., and Mishra, R. (2016) Galectin-9: From cell biology to complex disease dynamics, *Journal of biosciences 41*, 507-534.
22. Anderson, A. C., Anderson, D. E., Bregoli, L., Hastings, W. D., Kassam, N., Lei, C., Chandwaskar, R., Karman, J., Su, E. W., Hirashima, M., Bruce, J. N., Kane, L. P., Kuchroo, V. K., and Hafler, D. A. (2007) Promotion of tissue inflammation by the immune receptor Tim-3 expressed on innate immune cells, *Science 318*, 1141-1143.
23. Matsumoto, R., Matsumoto, H., Seki, M., Hata, M., Asano, Y., Kanegasaki, S., Stevens, R. L., and Hirashima, M. (1998) Human ecalectin, a variant of human galectin-9, is a novel eosinophil chemoattractant produced by T lymphocytes, *The Journal of biological chemistry 273*, 16976-16984.
24. Zhu, C., Anderson, A. C., Schubart, A., Xiong, H., Imitola, J., Khoury, S. J., Zheng, X. X., Strom, T. B., and Kuchroo, V. K. (2005) The Tim-3 ligand galectin-9 negatively regulates T helper type 1 immunity, *Nature immunology 6*, 1245-1252.
25. Arikawa, T., Saita, N., Oomizu, S., Ueno, M., Matsukawa, A., Katoh, S., Kojima, K., Nagahara, K., Miyake, M., Yamauchi, A., Kohrogi, H., and Hirashima, M. (2010) Galectin-9 expands immunosuppressive macrophages to ameliorate T-cell-mediated lung inflammation, *European journal of immunology 40*, 548-558.

26. Dardalhon, V., Anderson, A. C., Karman, J., Apetoh, L., Chandwaskar, R., Lee, D. H., Cornejo, M., Nishi, N., Yamauchi, A., Quintana, F. J., Sobel, R. A., Hirashima, M., and Kuchroo, V. K. (2010) Tim-3/galectin-9 pathway: regulation of Th1 immunity through promotion of CD11b+Ly-6G+ myeloid cells, *Journal of immunology 185*, 1383-1392.
27. Cao, A., Alluqmani, N., Buhari, F. H. M., Wasim, L., Smith, L. K., Quaile, A. T., Shannon, M., Hakim, Z., Furmli, H., Owen, D. M., Savchenko, A., and Treanor, B. (2018) Galectin-9 binds IgM-BCR to regulate B cell signaling, *Nature communications 9*, 3288.
28. Giovannone, N., Liang, J., Antonopoulos, A., Geddes Sweeney, J., King, S. L., Pochebit, S. M., Bhattacharyya, N., Lee, G. S., Dell, A., Widlund, H. R., Haslam, S. M., and Dimitroff, C. J. (2018) Galectin-9 suppresses B cell receptor signaling and is regulated by I-branching of N-glycans, *Nature communications 9*, 3287.
29. Santalla Mendez, R., Rodgers Furones, A., Classens, R., Fedorova, K., Haverdil, M., Canela Capdevila, M., van Duffelen, A., Spruijt, C. G., Vermeulen, M., Ter Beest, M., van Spriel, A. B., and Querol Cano, L. (2023) Galectin-9 interacts with Vamp-3 to regulate cytokine secretion in dendritic cells, *Cellular and molecular life sciences : CMLS 80*, 306.
30. Querol Cano, L., Tagit, O., Dolen, Y., van Duffelen, A., Dieltjes, S., Buschow, S. I., Niki, T., Hirashima, M., Joosten, B., van den Dries, K., Cambi, A., Figdor, C. G., and van Spriel, A. B. (2019) Intracellular Galectin-9 Controls Dendritic Cell Function by Maintaining Plasma Membrane Rigidity, *iScience 22*, 240-255.
31. Dai, S. Y., Nakagawa, R., Itoh, A., Murakami, H., Kashio, Y., Abe, H., Katoh, S., Kontani, K., Kihara, M., Zhang, S. L., Hata, T., Nakamura, T., Yamauchi, A., and Hirashima, M. (2005) Galectin-9 induces maturation of human monocyte-derived dendritic cells, *Journal of immunology 175*, 2974-2981.
32. Kageshita, T., Kashio, Y., Yamauchi, A., Seki, M., Abedin, M. J., Nishi, N., Shoji, H., Nakamura, T., Ono, T., and Hirashima, M. (2002) Possible role of galectin-9 in cell aggregation and apoptosis of human melanoma cell lines and its clinical significance, *International journal of cancer 99*, 809-816.
33. Iqbal, A. J., Krautter, F., Blacksell, I. A., Wright, R. D., Austin-Williams, S. N., Voisin, M. B., Hussain, M. T., Law, H. L., Niki, T., Hirashima, M., Bombardieri, M., Pitzalis, C., Tiwari, A., Nash, G. B., Norling, L. V., and Cooper, D. (2022) Galectin-9 mediates neutrophil capture and adhesion in a CD44 and beta2 integrin-dependent manner, *FASEB journal : official publication of the Federation of American Societies for Experimental Biology 36*, e22065.
34. Bourguignon, L. Y. (2008) Hyaluronan-mediated CD44 activation of RhoGTPase signaling and cytoskeleton function promotes tumor progression, *Seminars in cancer biology 18*, 251-259.
35. Katoh, S., Ishii, N., Nobumoto, A., Takeshita, K., Dai, S. Y., Shinonaga, R., Niki, T., Nishi, N., Tominaga, A., Yamauchi, A., and Hirashima, M. (2007) Galectin-9 inhibits CD44-hyaluronan interaction and suppresses a murine model of allergic asthma, *American journal of respiratory and critical care medicine 176*, 27-35.
36. Hsu, Y. L., Wang, M. Y., Ho, L. J., Huang, C. Y., and Lai, J. H. (2015) Up-regulation of galectin-9 induces cell migration in human dendritic cells infected with dengue virus, *Journal of cellular and molecular medicine 19*, 1065-1076.
37. de Vries, I. J., Eggert, A. A., Scharenborg, N. M., Vissers, J. L., Lesterhuis, W. J., Boerman, O. C., Punt, C. J., Adema, G. J., and Figdor, C. G. (2002) Phenotypical and functional characterization of clinical grade dendritic cells, *Journal of immunotherapy 25*, 429-438.
38. Shehwana, H., Kumar, S. V., Melott, J. M., Rohrdanz, M. A., Wakefield, C., Ju, Z., Siwak, D. R., Lu, Y., Broom, B. M., Weinstein, J. N., Mills, G. B., and Akbani, R. (2022) RPPA SPACE: an R package for normalization and quantitation of Reverse-Phase Protein Array data, *Bioinformatics 38*, 5131-5133.
39. Akbani, R., Becker, K. F., Carragher, N., Goldstein, T., de Koning, L., Korf, U., Liotta, L., Mills, G. B., Nishizuka, S. S., Pawlak, M., Petricoin, E. F., 3rd, Pollard, H. B., Serrels, B., and Zhu, J. (2014) Realizing the promise of reverse phase protein arrays for clinical, translational, and basic research: a workshop report: the RPPA (Reverse Phase Protein Array) society, *Molecular & cellular proteomics : MCP 13*, 1625-1643.
40. Siwak, D. R., Li, J., Akbani, R., Liang, H., and Lu, Y. (2019) Analytical Platforms 3: Processing Samples via the RPPA Pipeline to Generate Large-Scale Data for Clinical Studies, *Advances in experimental medicine and biology 1188*, 113-147.
41. Zhou, Y., Zhou, B., Pache, L., Chang, M., Khodabakhshi, A. H., Tanaseichuk, O., Benner, C., and Chanda, S. K. (2019) Metascape provides a biologist-oriented resource for the analysis of systems-level datasets, *Nature communications 10*, 1523.
42. van Rijn, A., Paulis, L., te Riet, J., Vasaturo, A., Reinieren-Beeren, I., van der Schaaf, A., Kuipers, A. J., Schulte, L. P., Jongbloets, B. C., Pasterkamp, R. J., Figdor, C. G., van Spriel, A. B., and Buschow, S. I. (2016) Semaphorin 7A Promotes Chemokine-Driven Dendritic Cell Migration, *Journal of Immunology 196*, 459-468.
43. Kolberg, L., Raudvere, U., Kuzmin, I., Adler, P., Vilo, J., and Peterson, H. (2023) g:Profiler-interoperable web service for functional enrichment analysis and gene identifier mapping (2023 update), *Nucleic acids research 51*, W207-W212.
44. Griss, J., Viteri, G., Sidiropoulos, K., Nguyen, V., Fabregat, A., and Hermjakob, H. (2020) ReactomeGSA - Efficient Multi-Omics Comparative Pathway Analysis, *Molecular & cellular proteomics : MCP 19*, 2115-2125.
45. Renkawitz, J., Schumann, K., Weber, M., Lammermann, T., Pflicke, H., Piel, M., Polleux, J., Spatz, J. P., and Sixt, M. (2009) Adaptive force transmission in amoeboid cell migration, *Nature cell biology 11*, 1438-1443.
46. Forster, R., Schubel, A., Breitfeld, D., Kremmer, E., Renner-Muller, I., Wolf, E., and Lipp, M. (1999) CCR7 coordinates the primary immune response by establishing functional microenvironments in secondary lymphoid organs, *Cell 99*, 23-33.
47. Meili, R., and Firtel, R. A. (2003) Two poles and a compass, *Cell 114*, 153-156.

48. Wu, C., Thalhamer, T., Franca, R. F., Xiao, S., Wang, C., Hotta, C., Zhu, C., Hirashima, M., Anderson, A. C., and Kuchroo, V. K. (2014) Galectin-9-CD44 interaction enhances stability and function of adaptive regulatory T cells, *Immunity 41*, 270-282.
49. Rahmati, A., Bigam, S., and Elahi, S. (2023) Galectin-9 promotes natural killer cells activity via interaction with CD44, *Frontiers in immunology 14*, 1131379.
50. Liu, J., Zhang, X., Cheng, Y., and Cao, X. (2021) Dendritic cell migration in inflammation and immunity, *Cellular & molecular immunology 18*, 2461-2471.
51. Imai, K., Minamiya, Y., Koyota, S., Ito, M., Saito, H., Sato, Y., Motoyama, S., Sugiyama, T., and Ogawa, J. (2012) Inhibition of dendritic cell migration by transforming growth factor-beta1 increases tumor-draining lymph node metastasis, *Journal of experimental & clinical cancer research : CR 31*, 3.
52. Villablanca, E. J., Raccosta, L., Zhou, D., Fontana, R., Maggioni, D., Negro, A., Sanvito, F., Ponzoni, M., Valentinis, B., Bregni, M., Prinetti, A., Steffensen, K. R., Sonnino, S., Gustafsson, J. A., Doglioni, C., Bordignon, C., Traversari, C., and Russo, V. (2010) Tumor-mediated liver X receptor-alpha activation inhibits CC chemokine receptor-7 expression on dendritic cells and dampens antitumor responses, *Nature medicine 16*, 98-105.
53. Pinho, S. S., Alves, I., Gaifem, J., and Rabinovich, G. A. (2023) Immune regulatory networks coordinated by glycans and glycan-binding proteins in autoimmunity and infection, *Cellular & molecular immunology 20*, 1101-1113.
54. Golden-Mason, L., McMahan, R. H., Strong, M., Reisdorph, R., Mahaffey, S., Palmer, B. E., Cheng, L., Kulesza, C., Hirashima, M., Niki, T., and Rosen, H. R. (2013) Galectin-9 functionally impairs natural killer cells in humans and mice, *Journal of virology 87*, 4835-4845.
55. Mansour, A. A., Raucci, F., Sevim, M., Saviano, A., Begum, J., Zhi, Z., Pezhman, L., Tull, S., Maione, F., and Iqbal, A. J. (2022) Galectin-9 supports primary T cell transendothelial migration in a glycan and integrin dependent manner, *Biomedicine & pharmacotherapy = Biomedecine & pharmacotherapie 151*, 113171.
56. Kasamatsu, A., Uzawa, K., Nakashima, D., Koike, H., Shiiba, M., Bukawa, H., Yokoe, H., and Tanzawa, H. (2005) Galectin-9 as a regulator of cellular adhesion in human oral squamous cell carcinoma cell lines, *International journal of molecular medicine 16*, 269-273.
57. Irie, A., Yamauchi, A., Kontani, K., Kihara, M., Liu, D., Shirato, Y., Seki, M., Nishi, N., Nakamura, T., Yokomise, H., and Hirashima, M. (2005) Galectin-9 as a prognostic factor with antimetastatic potential in breast cancer, *Clinical cancer research : an official journal of the American Association for Cancer Research 11*, 2962-2968.
58. Zhang, Z. Y., Dong, J. H., Chen, Y. W., Wang, X. Q., Li, C. H., Wang, J., Wang, G. Q., Li, H. L., and Wang, X. D. (2012) Galectin-9 acts as a prognostic factor with antimetastatic potential in hepatocellular carcinoma, *Asian Pacific journal of cancer prevention : APJCP 13*, 2503-2509.
59. Hittelet, A., Legendre, H., Nagy, N., Bronckart, Y., Pector, J. C., Salmon, I., Yeaton, P., Gabius, H. J., Kiss, R., and Camby, I. (2003) Upregulation of galectins-1 and -3 in human colon cancer and their role in regulating cell migration, *International journal of cancer 103*, 370-379.
60. Nagy, N., Bronckart, Y., Camby, I., Legendre, H., Lahm, H., Kaltner, H., Hadari, Y., Van Ham, P., Yeaton, P., Pector, J. C., Zick, Y., Salmon, I., Danguy, A., Kiss, R., and Gabius, H. J. (2002) Galectin-8 expression decreases in cancer compared with normal and dysplastic human colon tissue and acts significantly on human colon cancer cell migration as a suppressor, *Gut 50*, 392-401.
61. Hsu, D. K., Chernyavsky, A. I., Chen, H. Y., Yu, L., Grando, S. A., and Liu, F. T. (2009) Endogenous galectin-3 is localized in membrane lipid rafts and regulates migration of dendritic cells, *The Journal of investigative dermatology 129*, 573-583.
62. Thiemann, S., Man, J. H., Chang, M. H., Lee, B., and Baum, L. G. (2015) Galectin-1 regulates tissue exit of specific dendritic cell populations, *The Journal of biological chemistry 290*, 22662-22677.
63. Thiemann, S., and Baum, L. G. (2011) The road less traveled: regulation of leukocyte migration across vascular and lymphatic endothelium by galectins, *Journal of clinical immunology 31*, 2-9.
64. Zhang, W., Bhetwal, B. P., and Gunst, S. J. (2018) Rho kinase collaborates with p21-activated kinase to regulate actin polymerization and contraction in airway smooth muscle, *The Journal of physiology 596*, 3617-3635.
65. Szabo, K., Varga, D., Vegh, A. G., Liu, N., Xiao, X., Xu, L., Dux, L., Erdelyi, M., Rovo, L., and Keller-Pinter, A. (2022) Syndecan-4 affects myogenesis via Rac1-mediated actin remodeling and exhibits copy-number amplification and increased expression in human rhabdomyosarcoma tumors, *Cellular and molecular life sciences : CMLS 79*, 122.
66. Mayhew, M. W., Jeffery, E. D., Sherman, N. E., Nelson, K., Polefrone, J. M., Pratt, S. J., Shabanowitz, J., Parsons, J. T., Fox, J. W., Hunt, D. F., and Horwitz, A. F. (2007) Identification of phosphorylation sites in betaPIX and PAK1, *Journal of cell science 120*, 3911-3918.
67. Wang, Y., Sun, J., Ma, C., Gao, W., Song, B., Xue, H., Chen, W., Chen, X., Zhang, Y., Shao, Q., Wang, Q., Zhao, L., Liu, J., Wang, X., Wang, H., Zhang, Y., Yang, M., and Qu, X. (2016) Reduced Expression of Galectin-9 Contributes to a Poor Outcome in Colon Cancer by Inhibiting NK Cell Chemotaxis Partially through the Rho/ROCK1 Signaling Pathway, *PloS one 11*, e0152599.
68. Bi, S., Hong, P. W., Lee, B., and Baum, L. G. (2011) Galectin-9 binding to cell surface protein disulfide isomerase regulates the redox environment to enhance T-cell migration and HIV entry, *Proceedings of the National Academy of Sciences of the United States of America 108*, 10650-10655.
69. Bourguignon, L. Y., Wong, G., Earle, C., Krueger, K., and Spevak, C. C. (2010) Hyaluronan-CD44 interaction promotes c-Src-mediated twist signaling, microRNA-10b expression, and RhoA/RhoC up-regulation, leading to Rho-kinase-

associated cytoskeleton activation and breast tumor cell invasion, *The Journal of biological chemistry 285*, 36721-36735.

70. Yamauchi, A., Kontani, K., Kihara, M., Nishi, N., Yokomise, H., and Hirashima, M. (2006) Galectin-9, a novel prognostic factor with antimetastatic potential in breast cancer, *The breast journal 12*, S196-200.
71. Liang, M., Ueno, M., Oomizu, S., Arikawa, T., Shinonaga, R., Zhang, S., Yamauchi, A., and Hirashima, M. (2008) Galectin-9 expression links to malignant potential of cervical squamous cell carcinoma, *Journal of cancer research and clinical oncology 134*, 899-907.
72. Jeon, T. J., Gao, R., Kim, H., Lee, A., Jeon, P., Devreotes, P. N., and Zhao, M. (2019) Cell migration directionality and speed are independently regulated by RasG and Gbeta in Dictyostelium cells in electrotaxis, *Biology open 8*.
73. Kataoka, Y., Ohshio, Y., Teramoto, K., Igarashi, T., Asai, T., and Hanaoka, J. (2019) Hypoxia-induced galectin-3 enhances RhoA function to activate the motility of tumor cells in non-small cell lung cancer, *Oncology reports 41*, 853-862.

Figure 1

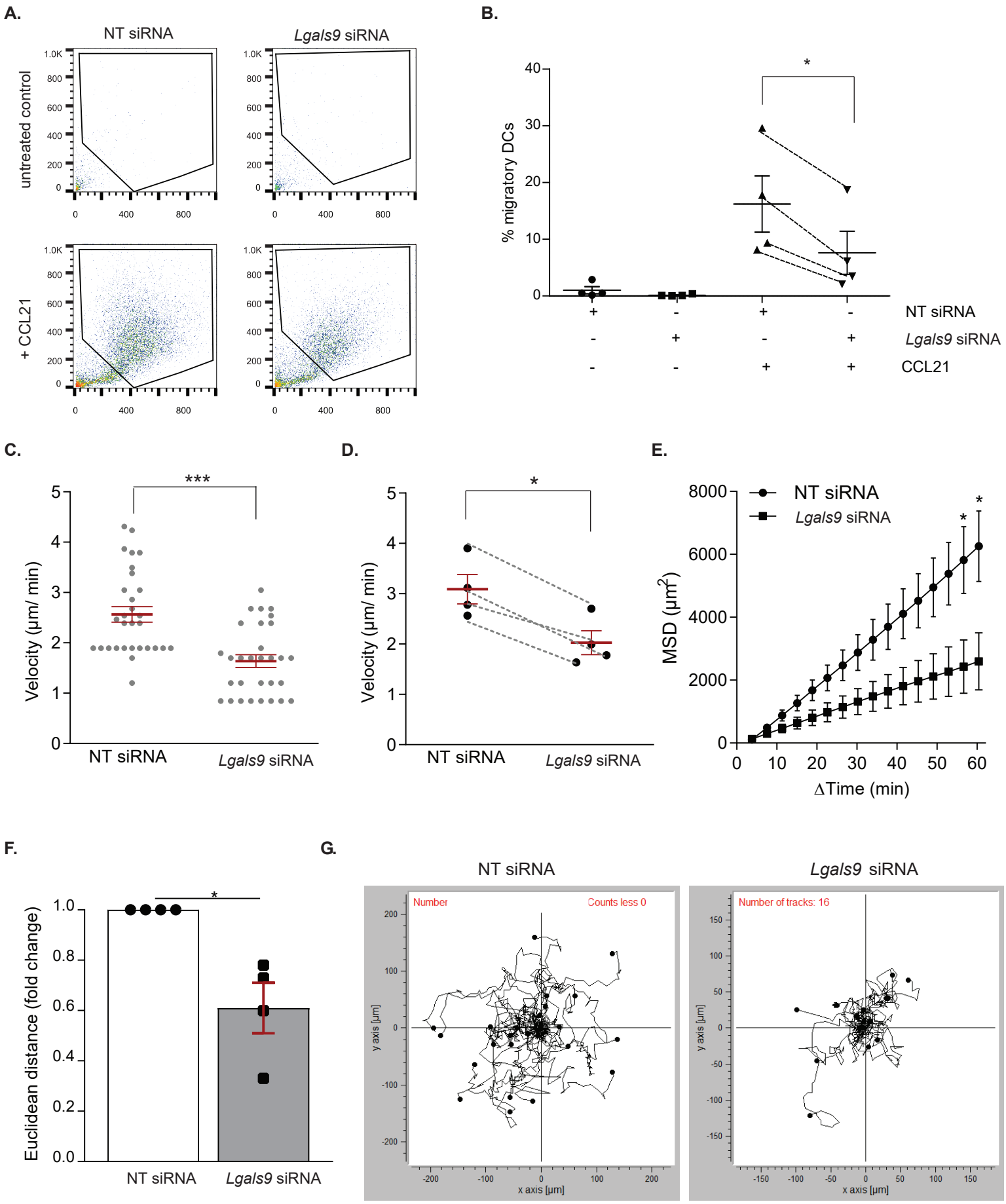
A.
NT siRNA
Lgals9 siRNA
untreated control
+ CCL21
B.
% migratory DCs
NT siRNA
Lgals9 siRNA
CCL21
C.
Velocity (µm/ min)
NT siRNA
Lgals9 siRNA
D.
Velocity (µm/ min)
NT siRNA
Lgals9 siRNA
E.
NT siRNA
Lgals9 siRNA
MSD (µm²)
ΔTime (min)
F.
Euclidean distance (fold change)
NT siRNA
Lgals9 siRNA
G.
NT siRNA
Lgals9 siRNA
Number
Counts less 0
Number of tracks: 16
x axis [µm]
y axis [µm]

Figure 2

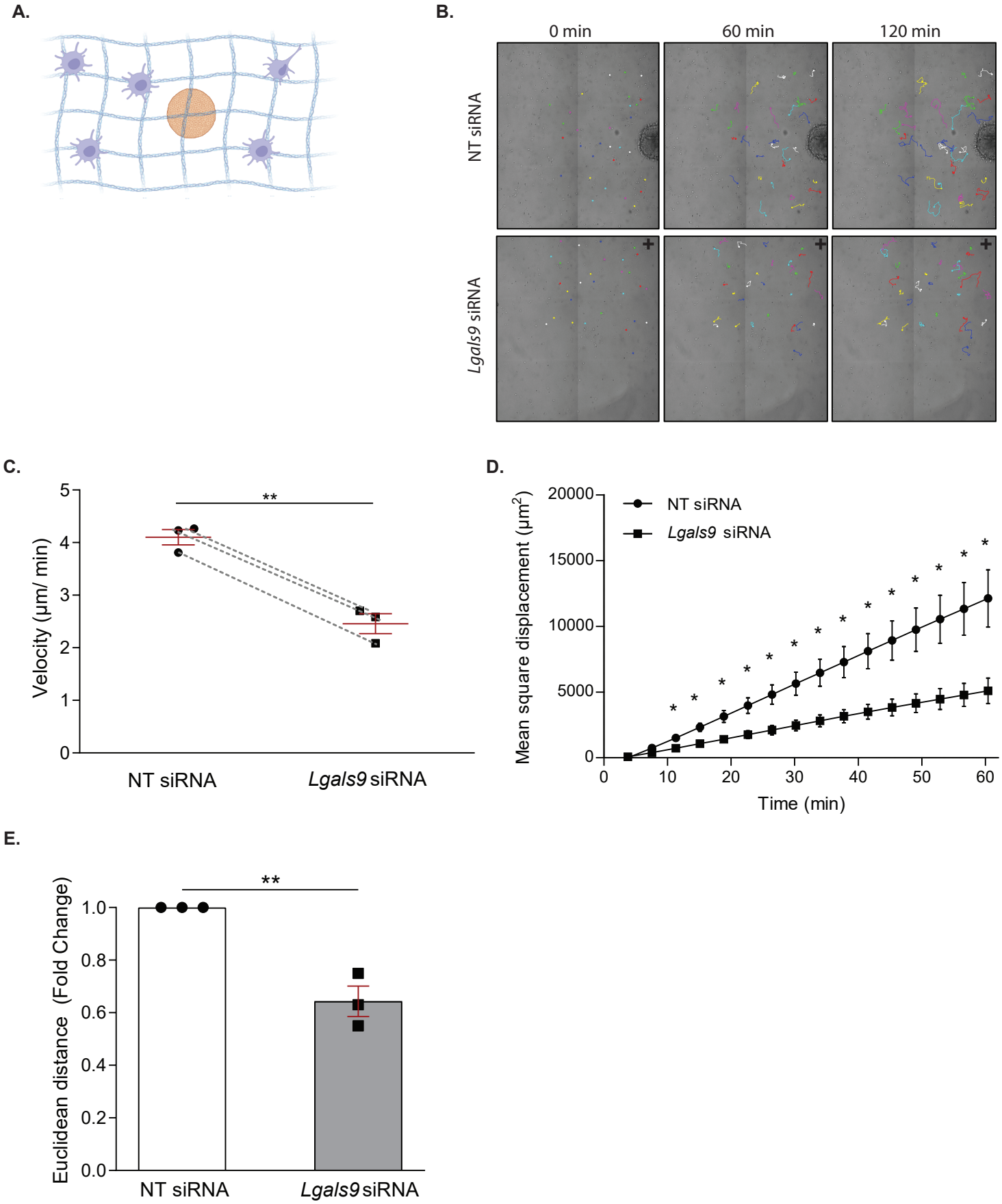
A.
B.
0 min
60 min
120 min
NT siRNA
Lgals9 siRNA
C.
Velocity (µm/ min)
**
NT siRNA
Lgals9 siRNA
D.
Mean square displacement (µm²)
NT siRNA
Lgals9 siRNA
Time (min)
E.
Euclidean distance (Fold Change)
**
NT siRNA
Lgals9 siRNA

Figure 3

A.

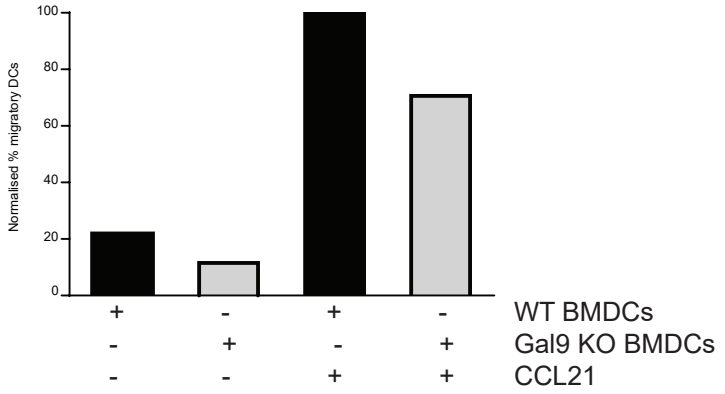

B.

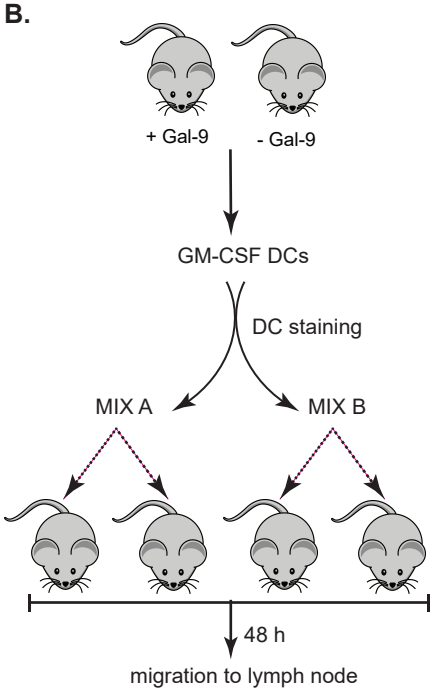

C.

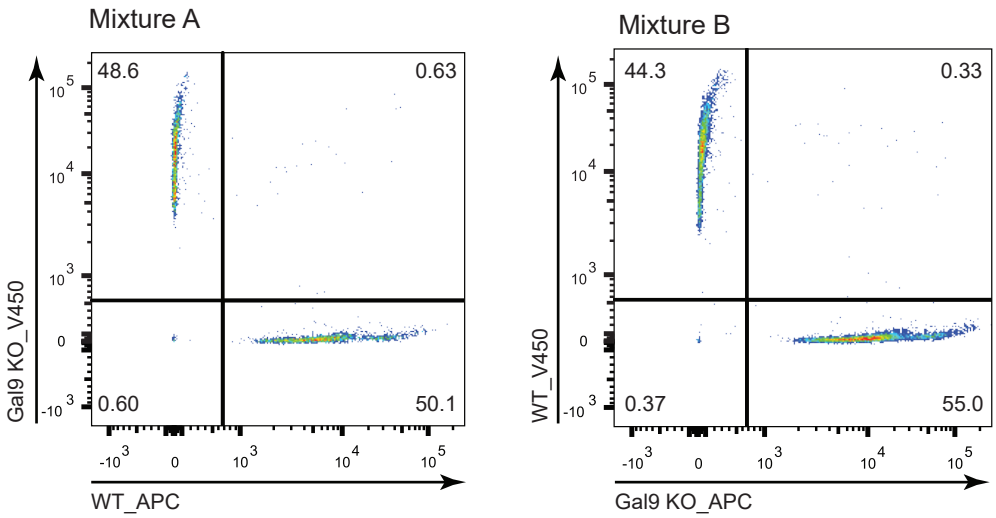

D.

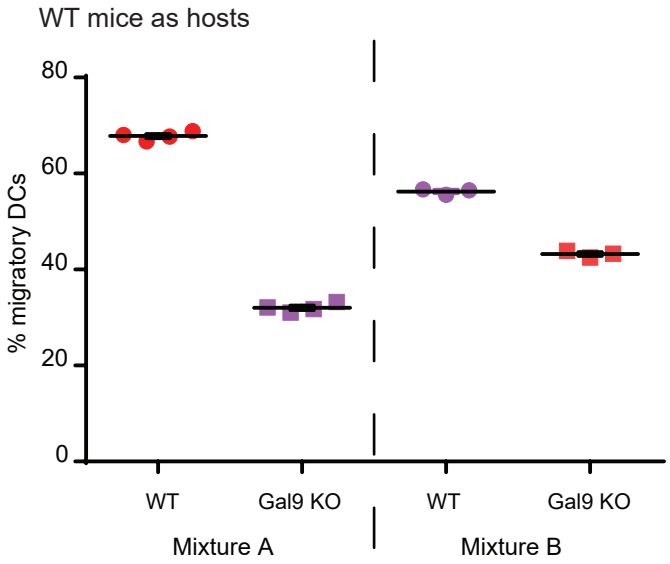

E.

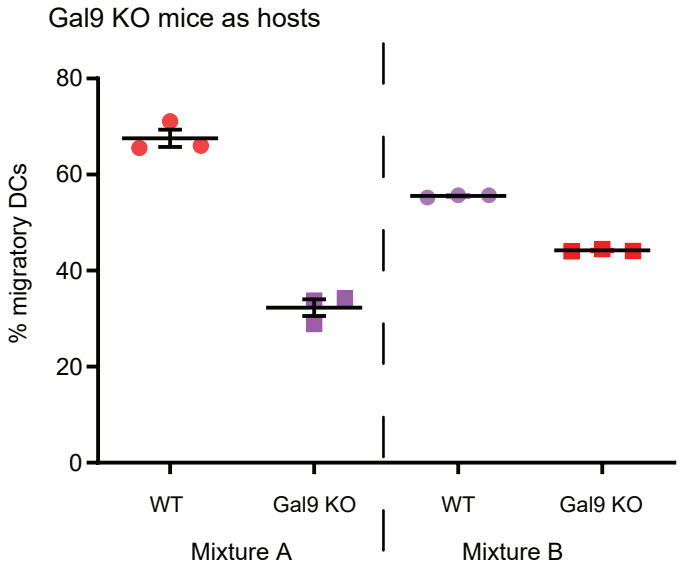

Figure 4

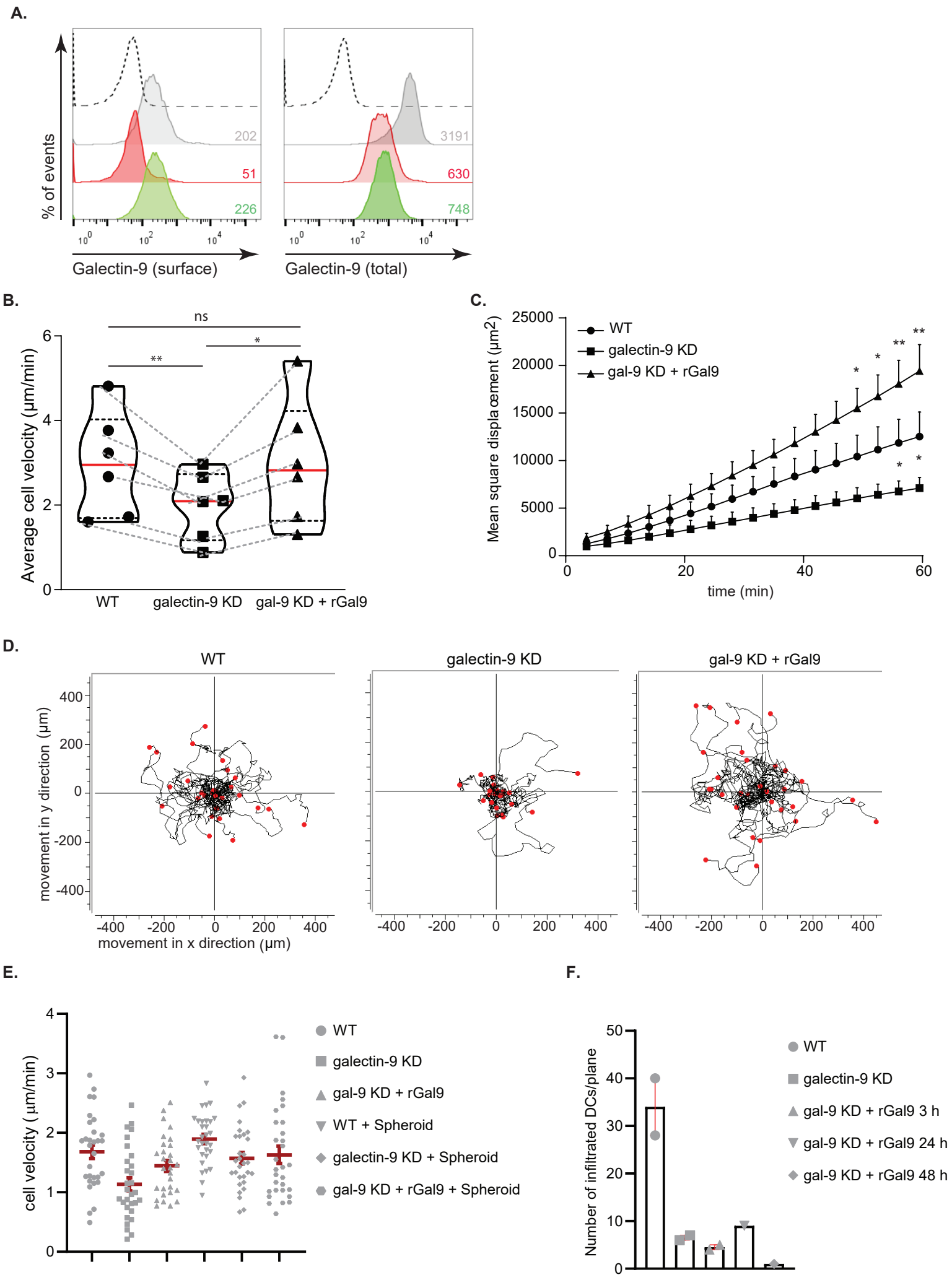
A.
% of events
202
51
226
3191
630
748
Galectin-9 (surface)
Galectin-9 (total)
B.
Average cell velocity (µm/min)
ns
*
**
WT
galectin-9 KD
gal-9 KD + rGal9
C.
Mean square displacement (µm2)
WT
galectin-9 KD
gal-9 KD + rGal9
time (min)
D.
WT
galectin-9 KD
gal-9 KD + rGal9
movement in y direction (µm)
movement in x direction (µm)
E.
cell velocity (µm/min)
WT
galectin-9 KD
gal-9 KD + rGal9
WT + Spheroid
galectin-9 KD + Spheroid
gal-9 KD + rGal9 + Spheroid
F.
Number of infiltrated DCs/plane
WT
galectin-9 KD
gal-9 KD + rGal9 3 h
gal-9 KD + rGal9 24 h
gal-9 KD + rGal9 48 h

Figure 5

A.

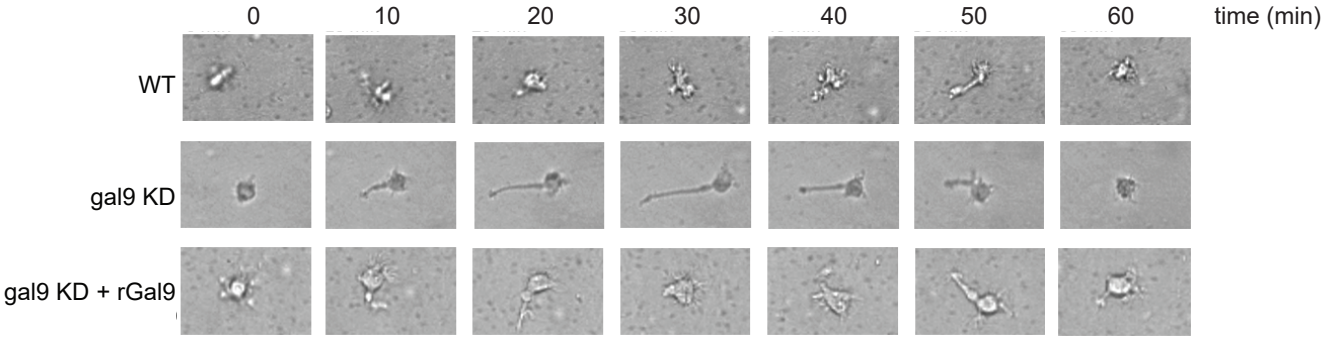

B.

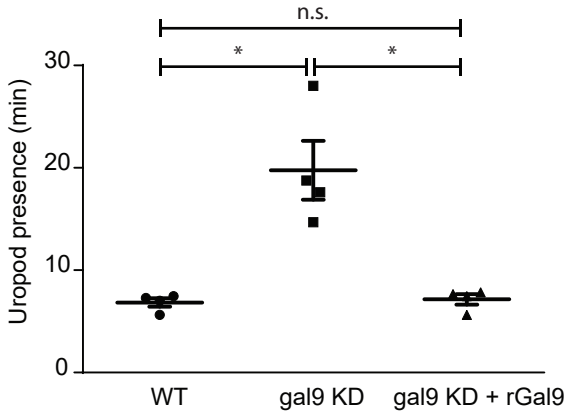

C.

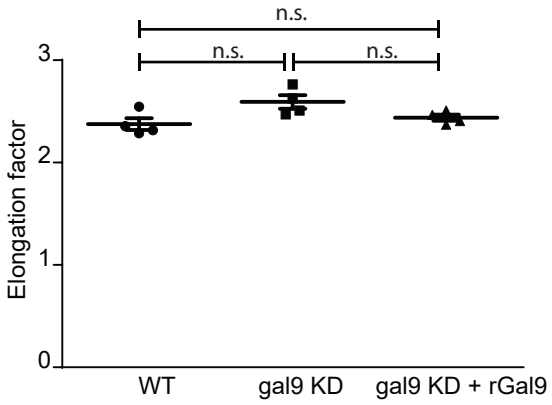

D.

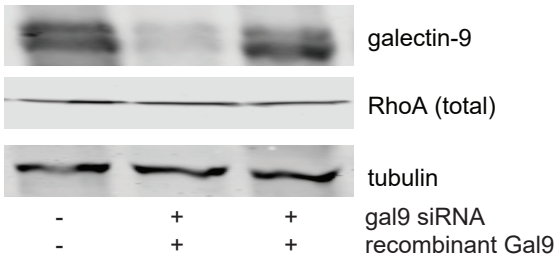

E.

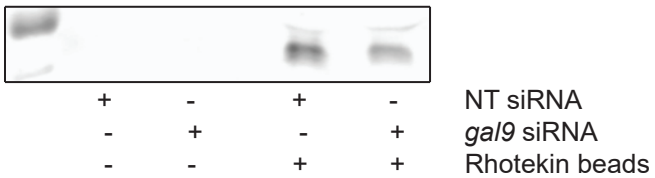

.

Figure 6

A.

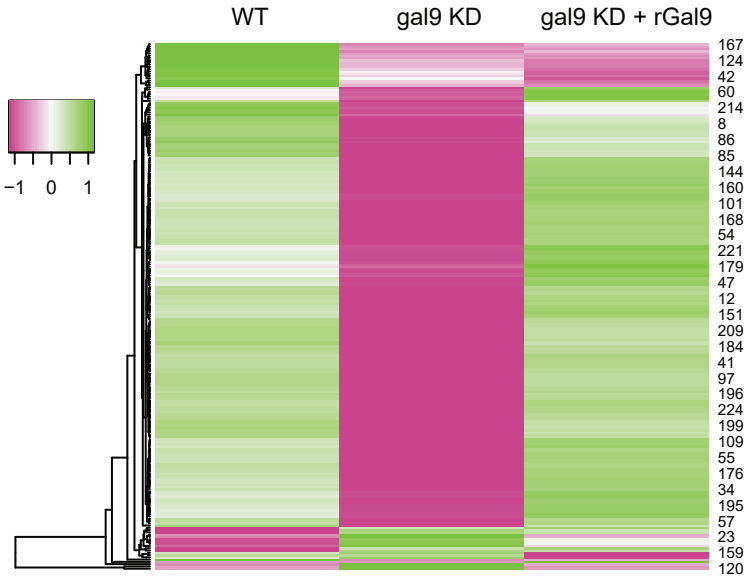

B.

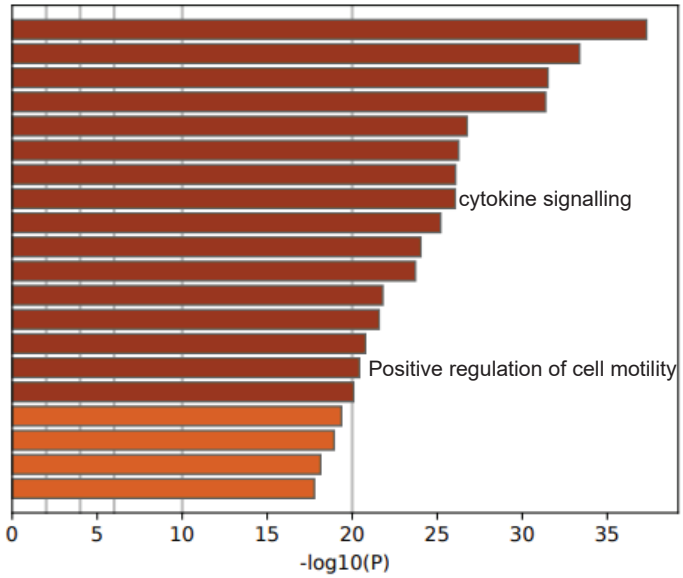

C.

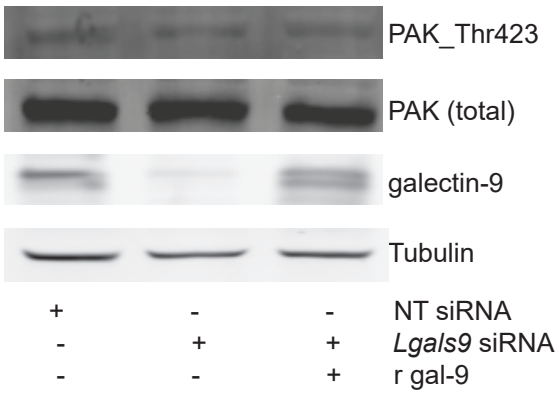

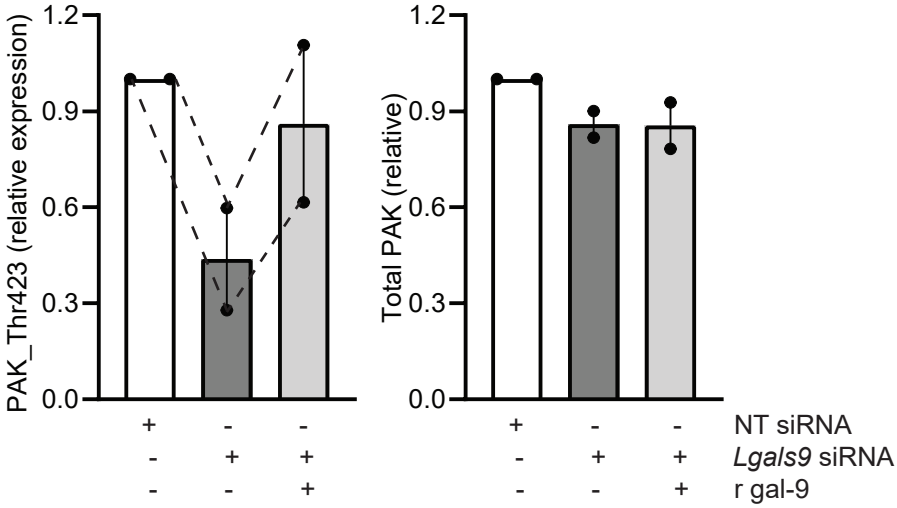

D.

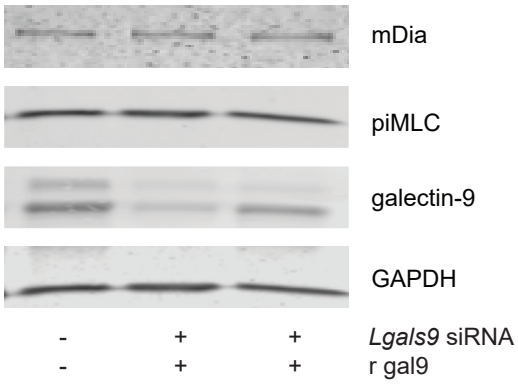

Figure 7

A.

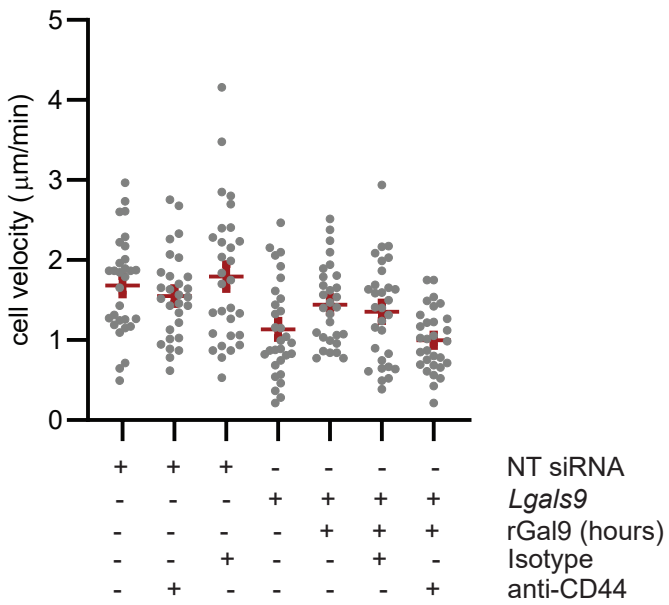
cell velocity (µm/min)
0
1
2
3
4
5
+ + + - - - - NT siRNA
- - - + + + + *Lgals9*
- - - - + + + rGal9 (hours)
- - + - - + - Isotype
- + - - - - + anti-CD44

B.

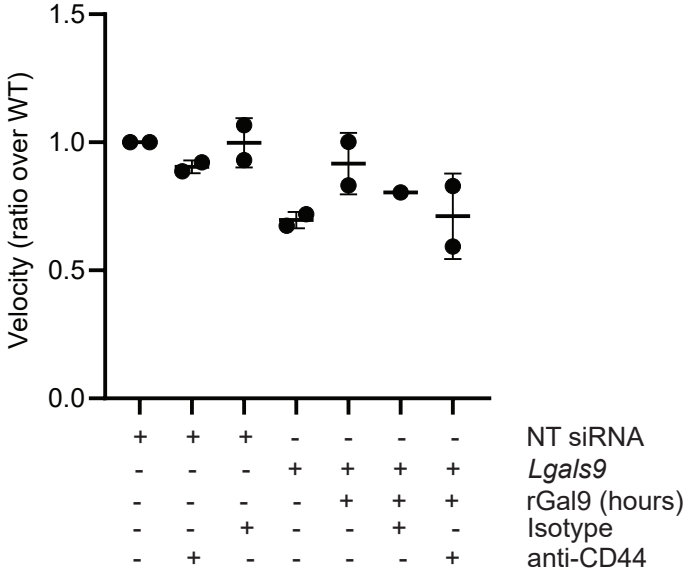
Velocity (ratio over WT)
0.0
0.5
1.0
1.5
+ + + - - - - NT siRNA
- - - + + + + *Lgals9*
- - - - + + + rGal9 (hours)
- - + - - + - Isotype
- + - - - - + anti-CD44

C.

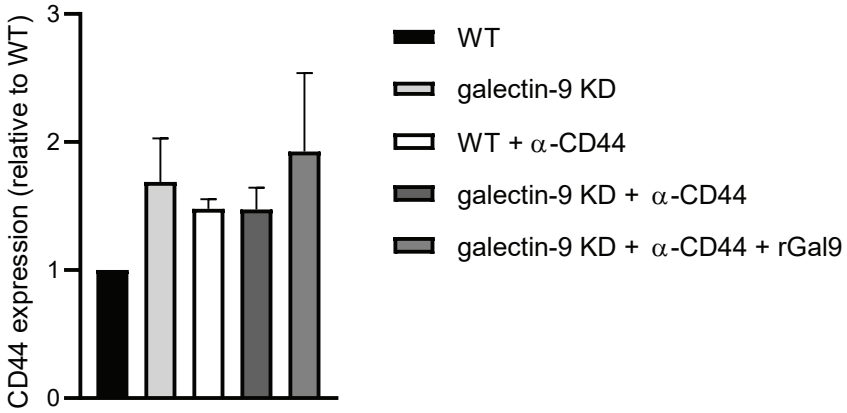
CD44 expression (relative to WT)
0
1
2
3
WT
galectin-9 KD
WT + α-CD44
galectin-9 KD + α-CD44
galectin-9 KD + α-CD44 + rGal9

Figure 8

A.

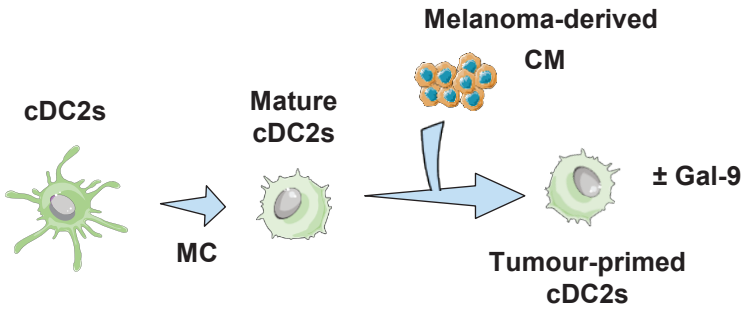

B.

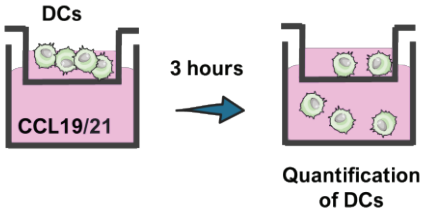

C.

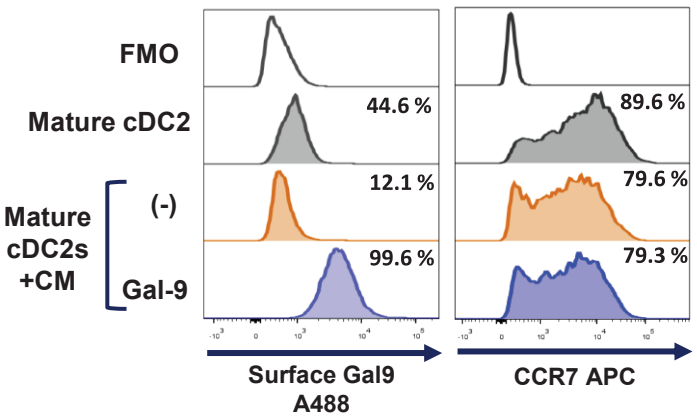

D.

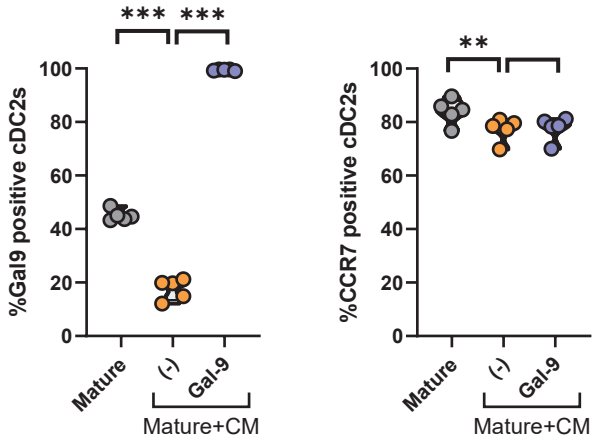
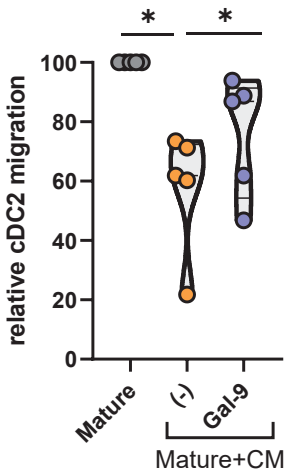
E.